AN ABSTRACT OF THE THESIS OF

Bradyn J. Wuth for the degree of Master of Science in Nuclear Engineering presented on May 30, 2014.

Title: Comparative Analysis of the Žukauskas Method and Data from the OSU MASLWR Test Facility Steam Generator

Abstract approved: _____

Qiao Wu

Some of the next generation of small modular reactors have been designed with helically coiled steam generators integrated into the reactor vessel to enhance natural circulation. According to the developers of TASS/SMR, a one-dimensional thermal hydraulic code written to model the Korean Atomic Energy Research Institute's SMART reactor, the Žukauskas correlation, a heat transfer correlation designed for banks of straight tubes in crossflow, accurately models the heat transfer into helical steam generator tubes. Data has been collected using the Oregon State University Multi-Application Small Light Water Reactor (MASLWR) Test Facility to test whether the Žukauskas correlation can accurately predict the helical steam generator heat transfer coefficients for a natural circulation driven reactor.

A one-dimensional, lumped parameter method was devised to use the limited instrumentation of the facility to calculate a temperature profile inside the tubes. From the calculated bulk fluid temperatures, wall temperatures were iteratively solved for and used to generate semi-local heat transfer coefficients. It was found that the instrumentation in the steam generator region of MASLWR Test Facility is too sparse to generate accurate heat transfer coefficients, but the calculated wall

temperatures can be averaged over the length of the tubes to find a good global wall temperature. This global wall temperature was used in a global analysis that found that the Žukauskas correlation works well when both systems are at high flow rates but becomes increasingly worse as the flow rates are lowered.

Comparative Analysis of the Žukauskas Method and Data from the OSU MASLWR Test Facility Steam Generator

by

Bradyn J. Wuth

A THESIS

submitted to

Oregon State University

in partial fulfillment of
the requirements for the
degree of

Master of Science

Presented May 30, 2014
Commencement June 2014

Master of Science thesis of Bradyn J. Wuth presented on May 30, 2014.

APPROVED:

Major Professor, representing Nuclear Engineering

Head of the Department of Nuclear Engineering and Radiation Health Physics

---

Dean of the Graduate School

I understand that my thesis will become part of the permanent collection of Oregon State University libraries. My signature below authorizes release of my thesis to any reader upon request.

Bradyn J. Wuth, Author

ACKNOWLEDGEMENTS

Thanks first and foremost to God who helped me through many hard and frustrating times over the last several years and who has taught me so much about myself and what life is truly about.

Thanks to all my family, friends, classmates, and coworkers who have encouraged and pushed me to grow both as a student and as a person.

A big thank you to all of the MASLWR testing team for their tireless work generating quality data and maintaining the facility. Thanks for being good friends over the last few years and for lots of fun times during long test days.

Finally thanks to Dr. Wu who gave me this opportunity and has guided me through the process of developing this thesis. I would never have been able to get this far without your steady encouragement and creative problem solving abilities. Whenever I found a problem that I could not solve you helped me understand and overcome it.

TABLE OF CONTENTS

Page

1 Introduction 1

1.1 Small Modular Reactors . . . 2
1.1.1 NuScale Power, Inc. . . . 5
1.1.2 Multi-Application Small Light Water Reactor . . . 8
1.2 Objectives . . . 10

2 Literature Review 11

2.1 Previous Work in Helical Coils . . . 11
2.2 TASS/SMR . . . 15
2.2.1 Steam Generator Correlations . . . 20

3 MASLWR Facility Description 24

3.1 MASLWR Facility . . . 24
3.1.1 Primary System . . . 25
3.1.2 Secondary System . . . 28
3.1.3 Containment and Cooling Pool Vessels . . . 31
3.2 Data Collection . . . 34
3.3 Synopsis of Testing . . . 34

4 Methods 36

4.1 Global Analysis . . . 36
4.2 Discretized Analysis . . . 37
4.2.1 Discretization . . . 38
4.2.2 Calculations & Methodology . . . 40
4.3 Updated Global Analysis . . . 57

5 Results & Discussion 58

5.1 Calculation Inputs . . . 58
5.2 Global Analysis . . . 62
5.3 Discretized Analysis . . . 63
5.3.1 End Cell Linear Heat Rate Assumption Validation . . . 72

TABLE OF CONTENTS (Continued)

Page

5.4 Updated Global Analysis 72
5.5 Correlation Substitution 75

6 Conclusions 80

Bibliography 82

LIST OF FIGURES

Figure		Page
1.1	Basic Rendering of a U-tube Heat Exchanger	3
1.2	Basic Rendering of a Helically Coiled Heat Exchanger	4
1.3	SMART Power Module	6
1.4	NuScale Power Plant Design	7
2.1	Secondary Flow in Curved Pipes	12
3.1	MASLWR Reactor Pressure Vessel Schematic	27
3.2	MASLWR Steam Generator Tubes Model	29
3.3	MASLWR Steam Generator, Top View	30
3.4	MASLWR Containment and Cooling Pool Vessels Schematic	32
4.1	Linear Heat Rate Through Chimney Wall	43
4.2	Transition Cell Heat Transfer Rate Redistribution	51
4.3	Transition Cell Heat Transfer Rate Redistribution	56
5.1	Primary Side Temperatures at Different Power Levels	61
5.2	Secondary Bulk Fluid Temperature at 392 kW	65
5.3	Secondary Bulk Fluid Temperature at 300 kW	65
5.4	Secondary Bulk Fluid Temperature at 200 kW	66
5.5	Secondary Bulk Fluid Temperature at 100 kW	66
5.6	Inner Tube Wall Temperature at 392 kW	67
5.7	Inner Tube Wall Temperature at 300 kW	67
5.8	Inner Tube Wall Temperature at 200 kW	68
5.9	Inner Tube Wall Temperature at 100 kW	68

LIST OF FIGURES (Continued)

Figure		Page
5.10	Heat Transfer Coefficients Calculated for 392 kW	70
5.11	Heat Transfer Coefficients Calculated for 300 kW	70
5.12	Heat Transfer Coefficients Calculated for 200 kW	71
5.13	Heat Transfer Coefficients Calculated for 100 kW	71
5.14	Inner Tube Wall Temperature at 392 kW	76
5.15	Inner Tube Wall Temperature at 300 kW	76
5.16	Inner Tube Wall Temperature at 200 kW	77
5.17	Inner Tube Wall Temperature at 100 kW	77
5.18	Heat Transfer Coefficients Calculated for 392 kW	78
5.19	Heat Transfer Coefficients Calculated for 300 kW	78
5.20	Heat Transfer Coefficients Calculated for 200 kW	79
5.21	Heat Transfer Coefficients Calculated for 100 kW	79

LIST OF TABLES

Table		Page
3.1	MASLWR Steam Generator Section Dimensions	26
3.2	Steam Tube Dimensions	26
3.3	Steam Generator Instrumentation	33
4.1	Steam Generator Heights	39
4.2	Steam Generator Tube Cell Lengths	39
4.3	Pre-Calculation Constants	40
5.1	Calculated Volume Values From OSU MASLWR Test Facility	59
5.2	Averaged Input Values From Test Data	59
5.3	Averaged Temperature Values From Test Data	60
5.4	Global Heat Transfer Coefficients Using Standard Temperature Differences Compared to the Žukauskas Correlation	62
5.5	Global Heat Transfer Coefficients Using Log-Mean Temperature Differences Compared to the Žukauskas Correlation	63
5.6	Error Caused by Linear Heat Rate Assumption	72
5.7	Average SG Tube Outside Wall Temperatures From the Discretized Analysis	73
5.8	Updated Global Heat Transfer Coefficients Using Standard Temperature Differences Compared to the Žukauskas Correlation	74
5.9	Updated Global Heat Transfer Coefficients Using Log-Mean Temperature Differences Compared to the Žukauskas Correlation	74

Chapter 1: Introduction

Industry is the lifeblood of the world economy today, and a very critical aspect of industrial processes is heat transfer. Every industry must consider heat transfer, whether just for safety and maintenance purposes or as part of their industrial processes. One of the largest uses of heat transfer technology today is heat exchangers. These come in many shapes and sizes. Boilers used for heating and refrigeration units are some of the simpler forms that they may take. Many chemical and petroleum production facilities, as well as all thermodynamic cycle based power generation plants, require the use of many different types of heat exchangers. Whether to heat or cool, vaporize or condense, devices are needed to efficiently transfer energy from one system to another.

There are many different configurations of heat exchangers that are used and studied today. Concentric tubes, plate, and finned are some of the generic types that have many different and specialized designs. The one that will be looked at in this study is known as a shell and tube type heat exchanger. The fundamental idea of the shell and tube is that one fluid flows through a tank, or shell, and over tubes that have another fluid flowing through them. Heat convection to the tube and conduction through the tube wall is the way that energy is transmitted between fluids. What distinguishes one shell and tube from another is the shape and design of the tubes themselves. Power generation is a field that uses many of these different types of shell and tube exchangers.

In power generation, the main function of a heat exchanger is to produce super heated steam to turn a turbine. Many nuclear pressurized water reactors (PWRs) today use a once-through or U-tube steam generator to transfer heat from the reactor coolant to a system with lower pressure so as to create steam for a turbine.

The once-through steam generator is true to its name; the water in the tubes passes through the hot shell section only once to boil it. U-tubes have tubes that make a U shape that allow the fluid in the tubes to take a longer route through the shell. This decreases the required length of the shell and frees up space in the reactor building. A relatively new concept for power applications that has been used for years in chemical production is helically shaped heat exchangers. In Figure 1.1 and Figure 1.2, one can see the differences between U-tube and helical exchangers. Helically coiled tubes allow for even longer tubes to be fit into smaller shells and they also increase the heat transfer because of flows internal to the tubes. This makes them more efficient as well. Another added benefit to helical coils over U-tubes is their resistance to thermal stresses. Due to the circular nature of the tubes, they are limited in their expansion and wear, whereas U-tubes must preferentially expand in the axial direction which can cause wear against other tubes or tube spacers. These qualities make helically coiled tubes ideal for the next generation of nuclear power plants.

1.1 Small Modular Reactors

One of the largest groups interested in helical heat exchangers are companies designing Small Modular Reactors (SMRs). SMRs are a new genre of nuclear reactor design that are typically smaller, safer, and more economical than the large power plants in operation currently; many SMRs have an integrated reactor vessel design that incorporates the reactor, steam generator, and pressurizer components into one vessel as opposed to several. This idea eliminates a major safety hazard that plagues the design of other power plants. This safety hazard is known as a Large Break Loss of Coolant Accident (LBLOCA) because there are no primary coolant lines from one component to another. During a LBLOCA, the system loses massive amounts of coolant, and once the nuclear core is uncovered, there is the possibility of a meltdown occurring. Smaller plants also allow for "scaling," which means that they can be built in groups in order to provide just the right amount of electricity

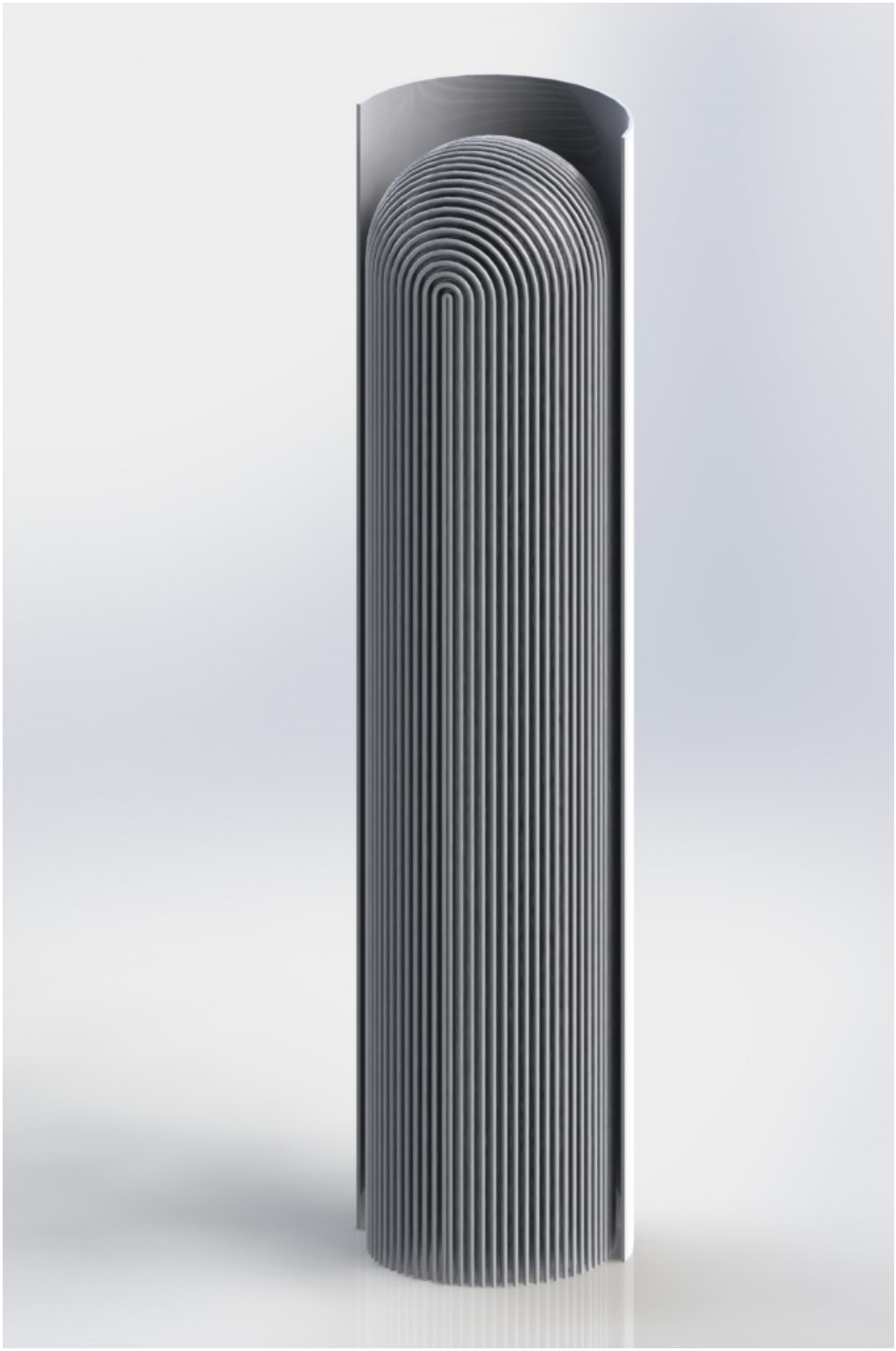

Figure 1.1: Basic Rendering of a U-tube Heat Exchanger

Figure 1.2: Basic Rendering of a Helically Coiled Heat Exchanger

for their area as opposed to one large plant that might produce too much energy now, but not enough in the future. A scaled approach allows for future growth as well. One of the design companies capitalizing on the scaled approach is NuScale Power, Inc.

The Korean Atomic Energy Research Institute is also developing an SMR known as SMART (System-integrated Modular Advanced ReacTor). It is designed to produce 330 MWt of power and has eight integrated steam generator cassettes that have helically coiled tubes which can be seen in Figure 1.3. SMART uses pumps to force the coolant around the system. This makes the heat transfer more efficient and helps maintain cooling during startup and shutdown operations, but it also provides another system to fail in accident scenarios. [1] Some designs have been transitioning to natural circulation operations so that they can eliminate the safety concerns and maintenance issues that arise when pumps are needed for reactor coolant flow. The NuScale design is capitalizing on this safety feature as well.

1.1.1 NuScale Power, Inc.

The NuScale Power plant is designed such that up to twelve of their reactors, or modules, can be placed in one large cooling pool and operated from one control room. This approach can be very economical because once the reactor building is finished, a few modules can be installed, produce power, and recoup some of the cost while building the other power modules. A conceptual drawing of the power plant is shown in Figure 1.4. Each module has its own containment vessel, and internal to the containment is the reactor vessel. The flow in the reactor is driven by natural circulation caused by the low core that heats water which rises through a chimney. Once at the top the water then comes down past a helical steam generator which cools the water and forces it down back to the core. The pressurizer is in the top-most section of the reactor vessel and is separated from the

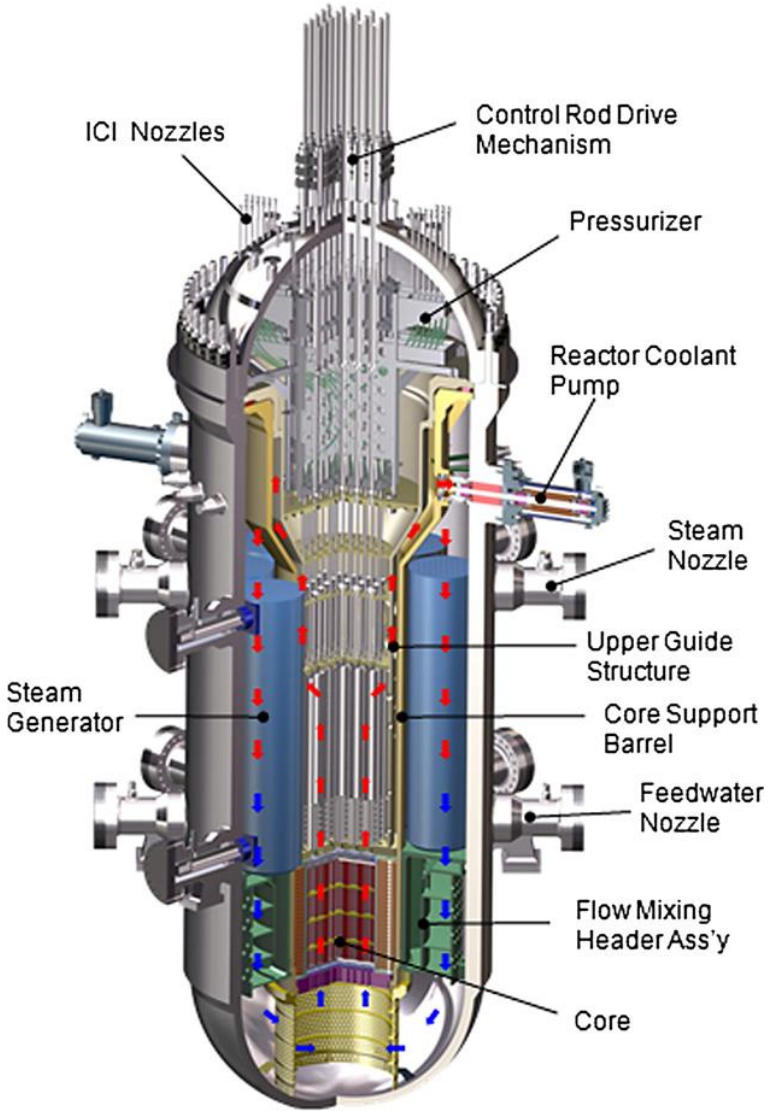

Figure 1.3: SMART Power Module

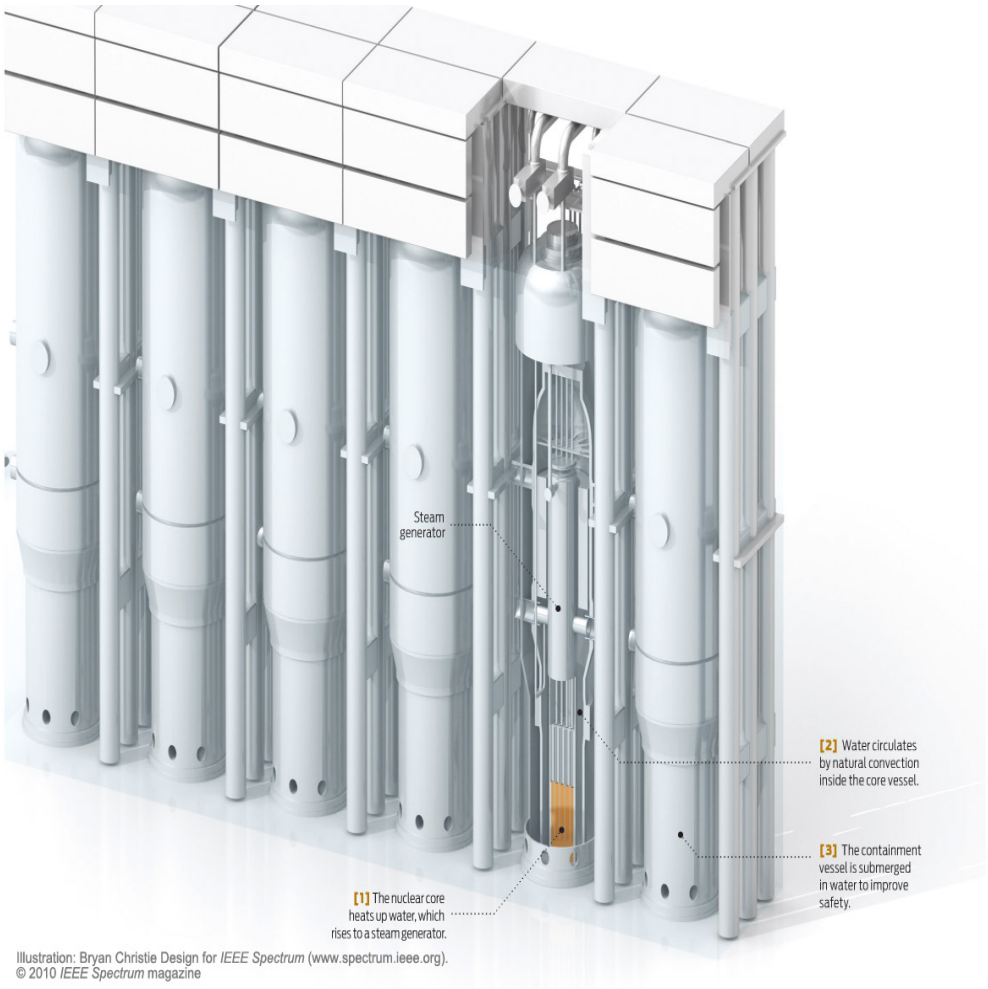

Figure 1.4: NuScale Power Plant Design

flow by a baffle plate that allows for thermal hydraulic communication between the pressurizer and the rest of the vessel. Outside of the main reactor building are the turbine buildings that receive the steam, turn the turbine to produce energy, and condense the steam before returning the water to the module for steam generation. Each module has its own turbine system associated with it so that each pair can be run independently of other module pairs.

Safety and scalability are, as mentioned before, the two main factors in NuScale's favor. With an integrated design, the LBLOCA is no longer an issue; only smaller breaks (SBLOCA) need to be studied during their safety analysis. Other accident scenarios, such as loss of on-site or off-site power, steam generator tube rupture, and turbine trips to name a few, must still be considered as well. Another accident that does not effect the NuScale design is primary coolant pump failure because it is all driven by natural circulation. Since there are no reactors like this in existence today, the licensing process through the Nuclear Regulatory Commission (NRC) will be very difficult. While the licensing process is going to take several years and a large amount of capital, NuScale was very fortunate to be a recipient of a grant from the Department of Energy (DOE). This has allowed a small startup company to become a competitor in the future energy business. The first major hurdle for NuScale will be to get their design licensed. To get their license, NuScale must validate computer models to show that their design is safe and reliable. The validation of the models comes from data gathered at facilities like the one described below.

1.1.2 Multi-Application Small Light Water Reactor

The NuScale design was birthed from a test facility designed by the Idaho National Engineering and Environmental Laboratory (INEEL), Nexant-Bechtel, Inc., and Oregon State University (OSU) known as the Multi-Application Small Light Water Reactor (MASLWR) Test Facility. The facility was a proof-of-concept test for the

feasibility of natural circulation reactors built under a grant from the DOE. The MASLWR Test Facility is scaled down in size and has electric heater rods instead of a nuclear core. The facility is built with the reactor vessel (RPV) external to the containment (HPC) and cooling pool vessels (CPV). It was designed that way to make maintenance more simple, but it also loses some modeling fidelity because there is no model of heat transfer between the RPV and the HPC.

The electric core in the RPV heats the water and causes it to rise up a chimney. At the end of the chimney, the flow is turned around by a baffle plate and flows down around the outside of the chimney and steam generator (SG). Once it reaches the bottom of the vessel, it is returned to the core and circulation continues. The SG is composed of 14 tubes that enter the vessel and then coil helically around the top portion of the chimney before exiting into a steam drum to be vented to atmosphere. Four of the tubes comprise the inner bank while five make up both the middle and outer banks. Greater design detail will be given in the Methods chapter.

Through testing at the facility, NuScale will be given data that proves the effectiveness of natural circulation as well as the response of the system to SBLOCAs and other accident scenarios like long term loss of cooling accidents. An SBLOCA is modeled by opening valves near the top or bottom of the vessel when at operating temperature and pressure and allowing flow to go through a nozzle that is properly scaled and into the containment vessel. The steam then condenses on the heat transfer plate (HTP) that simulates the heat transfer through the containment wall and into the cooling pool. Once enough steam has condensed, other valves can be opened to achieve circulation through the reactor core and containment vessel. This allows for continuous removal of the decay power from the core by dumping heat to the cooling pool. A long term cooling accident is simulated by draining the cooling pool and operating the core at very low powers to simulate the heat from nuclear decay. All of the valves used during the SBLOCA are opened, and the circulation caused by air cooling is recorded by the data acquisition system.

1.2 Objectives

An extensive amount or research has been done to study heat transfer in many different geometries, but little has been done on banks of helical coils. The objective of this study is to explore the heat transfer correlation used in a thermal hydraulic code written by developers at the Korean Atomic Energy Research Institute (KAERI), known as TASS/SMR, to simulate the heat transfer from an external flow to a helical steam generator and to see if it would be applicable to other similar systems through the use of data from the Multi-Application Small Light Water Reactor Test Facility at Oregon State University. With data from the facility, a heat transfer coefficient (HTC) can be approximated in several different ways and compared with the expected coefficient given by the correlation used in TASS/SMR.

Chapter 2: Literature Review

A review of relevant literature will be given in this section. It will include previous research into the use and understanding of helical coils and the special phenomena that occur when they are utilized as well as information on the TASS/SMR code that was developed by KAERI. Detailed explanations of all of the relevant correlations used in TASS/SMR and this paper's analysis will be given to help in the understanding of the later described methodology.

2.1 Previous Work in Helical Coils

D. Jeschke performed the first recorded experiments on curved tubes in 1925. With his data, he found an empirical formula for heat transfer to turbulent flow inside helical tubes that is still used by some today [2]. The first theoretical analysis was done by W.R. Dean in 1927. In his papers, Dean characterized the secondary flow inherent to curved tubes and its effect on heat transfer and pressure drop for laminar flows by solving the Navier-Stokes equations. [3, 4] With this information a parameter known as the Dean Number (Dn) has been used by many subsequent authors to quantify the differences between straight and curved pipes. The Dean number is traditionally represented as a function of Reynold's Number, tube radius (a), and the coil radius (R).

$$Dn = Re\sqrt{\frac{a}{R}} \tag{2.1}$$

The secondary flow that Dean identified is what gives helical coils such good heat transfer properties. As fluid moves through a curved section of pipe, the

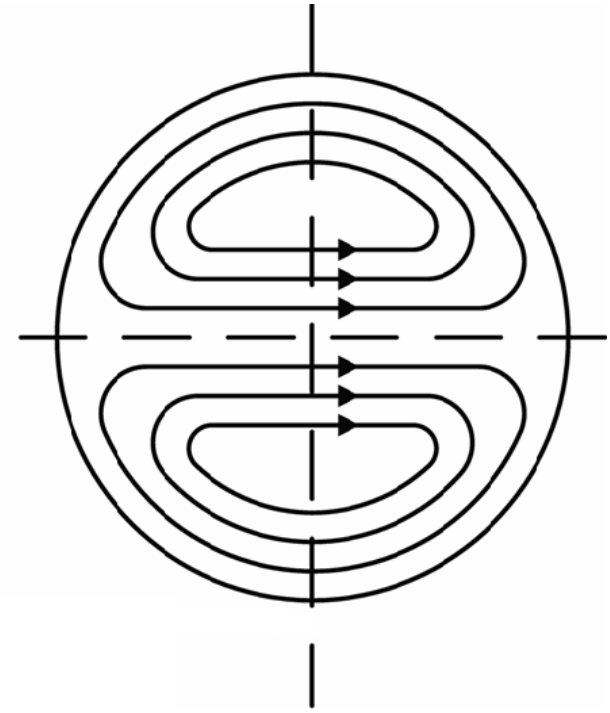

Figure 2.1: Secondary Flow in Curved Pipes

centripetal force of the tube wall on the fluid causes the flow to separate on the curve's outside edge and flow around the tube wall until it is pulled back into the core region on the inside edge of the curve. This creates two traveling spirals that appear as Figure 2.1 in the cross-section of the tube.

In the 1960s, many researchers began to investigate curved pipes and helical coils for their application in chemical processes. Ito [5] took Dean's analytical work and expanded it to find friction factors at larger Dean Numbers. His analytical and empirical expressions for friction factors are often used today when dealing with curved pipes. Since Ito covered the friction in curved tubes so well, many other authors look to his work to start their analysis for the heat transfer in helical coils.

Seban and McLaughlin [6] began their work to characterize the heat transfer in helical coils in 1962. They set up two coils for testing: one with a coil to tube diameter of 17 and the other 104. Using oil for laminar flows and water for turbulent flows, Seban and McLaughlin were able to generate heat transfer correlations for both laminar and turbulent flows. They found that laminar flows have a thermal entry effect that they could not account for, but after the entry length they were able to solve for a correlation. During their turbulent analysis there was no thermal entry length, and they were able to find an accurate correlation for the heat transfer. This turbulent correlation is used extensively when calculating heat transfer in helical coils and is given below.

$$Nu = 0.023 Re^{0.85} Pr^{0.4} \left(\frac{d_i}{D_c} \right)^{0.1} \tag{2.2}$$

Where Nu is the Nusselt Number ($\frac{hd_i}{k}$), Pr is the Prandtl Number ($\frac{c_p \mu}{k}$), and $\frac{d_i}{D_c}$ is the ratio of tube to coil diameters. Another researcher who looked at the laminar flow regime was E.F. Schmidt [7] in 1967. Schmidt's empirical formula also gives the Nu as a function of Re, Pr, and the diameter ratio.

$$Nu = 3.65 + 0.08\left[1 + 0.8\left(\frac{r}{R}\right)^{0.9}\right] \cdot Re^{\left[0.5+0.2903\left(\frac{r}{R}\right)^{0.194}\right]} \cdot Pr^{1/3} \tag{2.3}$$

Following in the footsteps of Dean, Ito, Seban, and McLaughlin another pair of researchers did an even more detailed study. Mori and Nakayama [8, 2] began with the theoretical studies done prior to their work and calculated the flow fields for both the laminar and turbulent regions in separate papers. By using their flow field analysis and data from other papers, Mori and Nakayama were able to find friction factor and heat transfer correlations that cover a large amount of fluid properties. In their second paper, the one on turbulent flows, they found two equations for heat transfer: one for gases ($Pr < 1$) and one for liquids ($Pr > 1$).

$$Nu = \begin{cases} \frac{1}{26.2}\frac{Pr}{Pr^{2/3}-0.074}Re^{4/5}\left(\frac{d_i}{D_c}\right)^{1/10}\left\{1 + \frac{0.098}{\left[Re(d_i/D_c)^2\right]^{1/5}}\right\} & \text{(for gases)} \\ \frac{1}{41.0}Re^{5/6}Pr^{0.4}\left(\frac{d_i}{D_c}\right)^{1/12}\left\{1 + \frac{0.061}{\left[Re(d_i/D_c)^{2.5}\right]^{1/6}}\right\} & \text{(for liquids)} \end{cases} \tag{2.4}$$

For all of these cases discussed, and many others not mentioned, the correlations were made for single-phase fluids. Less research has been done to quantify the heat transfer properties of two-phase boiling in helical coils. Much of the work done in helical two-phase flows is to characterize the departure from nucleate boiling so that they can find where the tube wall dries out and the heat transfer decreases rapidly. Owhadi et. al. [9] decided that information was needed on the heat transfer coefficient in boiling coils so they set up an experiment to gather data. Similar to many heat transfer test assemblies, Owhadi et. al. built coils that were heated by passing an electrical current through the tube wall, and a slew of pressure and temperature sensors were connected all around it. By pumping pre-heated water into the coil and measuring the temperature and pressure differ-

ences throughout it, they were able to find that turbulent boiling flows in coils are not very different from those in straight pipes. Upon analyzing the data, Owhadi and his fellow researchers found that the boiling heat transfer coefficient followed Chen's correlation [10] for straight pipe boiling within 15% over the entire quality range.

The other section of helical coil heat transfer that has had little quality analysis has been the part that deals with the external part of the coils. Some analysis has been done for heat transfer from helical coils to pools (Prabhanjan et. al. [11]), but it is not very useful for this project. One paper was found from the Ukrainian researchers Kanevets and Politykina [12] that tries to correct a straight tube bundle correlation for coiled bundles in crossflow. The correlation that they were trying to correct was originally found through experimental analysis by Žukauskas [13]. The Žukauskas correlation is given below.

$$Nu = CRe^{m}Pr^{0.36}\left(\frac{Pr_f}{Pr_w}\right)^{0.25} \tag{2.5}$$

In this equation, C and m are coefficients that are based off the Reynold's Number. Kanevets and Politykina found that the Žukauskas correlation already calculated the heat transfer fairly well for their experiments but also solved for an empirical correction factor that greatly improved the accuracy of the correlation over their limited set of data. Without a broader range of data, though, little can be concluded from their analysis.

2.2 TASS/SMR

KAERI has been developing the TASS/SMR code since the early 2000s to be the thermal hydraulic system code for the safety analysis of their SMART reactor. TASS/SMR stands for Transient and Set point Simulation/System-integrated

Modular Reactor code. It is a lumped parameter code that uses the finite volume method in a one-dimensional geometry and six conservation equations to model the reactor's entire set of operating conditions. The conservation equations include three mass equations (mixture, liquid, and non-condensable gas), two energy equations (mixture and steam), and a mixture momentum equation. Similar to many one-dimensional codes, TASS/SMR uses control volume nodes with flow path connectors to structure the systems. The nodes contain volume properties like mass and energy while the flow paths have no flow paths have no volume and, therefore, only represents the fluid's momentum. [14]

As with any code used for safety analysis, TASS/SMR has undergone many different verification tests to prove the validity of its results. It was first tested against simple, known problems. These tests included a manometric oscillation problem, a natural circulation problem, and a stratified flow problem along with several others [14]. The next phase of testing was to test TASS/SMR against other codes. Since TASS/SMR was built to model the SMART reactor, it was modeled both in TASS/SMR and another code from KAERI known as MARS. MARS is a compilation of the RELAP5/MOD3.2 and COBRA-TF codes. It was found that TASS/SMR calculated very similar values to MARS except for the pressurizer pressure. This was found to be because TASS/SMR uses a thermal equilibrium model that cannot handle non-homogeneous temperatures and could not predict the pressure increase. This perceived deficiency is not necessarily a bad thing because lower pressures are more conservative when calculating the departure from nucleate boiling ratio. [15]

Once any given code proves that it compares well with a standard, it must be proven to model reality. To validate the model, physical tests, known as separate effects tests, need to be done to show that each specific function of the code works accurately. Two of the primary separate effects tests were used to characterize the helical steam generator cassettes [14] and the core heat transfer models [16].

The steam generator was tested by building an experimental test facility that housed a single cassette prototype. Twenty-four steady state tests were performed by varying the primary side inlet temperature, primary side flow rate, secondary side inlet temperature, secondary side flow rate, and secondary side pressure. It was found that, similar to the comparison with the MARS code, calculated primary side pressure was low for tests with lower primary flow rates. TASS/SMR also calculates a secondary side exit temperature that was higher than the experimental values. These two errors did not appear to affect the heat transfer rate to the secondary side.

Another test facility known as VISTA (Experimental Verification by Integral Simulation of Transients and Accidents) was also used for steam generator testing. VISTA is a scaled down version of the reactor, similar to the MASLWR Test Facility, that was used to do integral effects test for the SMART reactor as its name suggests. Similar results were found in the sixteen steady state VISTA experiments as with the prototype cassette. The primary pressure was calculated lower than the experiments and secondary side outlet temperatures were calculated higher than the experiments, but again, higher flow rates proved to be more accurate. The developers attribute these errors to conservative assumptions made in the code.

The core heat transfer models were tested by comparing the code's calculation to published experimental data from other groups. The first comparison was to Bennett's heated tube tests published in 1976. In these tests, water was pumped up through a single, long, electrically heated tube to measure the critical heat flux location in the tube. Three tests were considered: a low mass and heat flux case, a medium mass and heat flux case, and a high mass and heat flux case. It was found in all cases that the wall temperature was calculated very well in the pre-critical heat flux region, but that the predicted location of the critical heat flux was lower than the experimental values for all cases. The temperatures in the post-critical heat flux regions were all conservatively high. The other data used for the verification of the core models was from Oak Ridge National Lab's

Thermal-Hydraulic Test Facility (THTF) which conducts steady state film boiling tests using a full-size electrically heated fuel bundle. Five tests with a range of conditions were run in TASS/SMR and found to predict the surface temperatures conservatively in all cases except for the low pressure, heat flux, and mass flux conditions.

The SBLOCA testing was also done at an integral effects test facility. It is known as the LOFT (loss of fluid test) facility. LOFT is a semi-scaled test facility that was designed purely to perform LOCA tests for traditional PWRs. Using quick-opening valves in a simulated hot and cold leg, different-sized LOCA events can be simulated. The verification test done for TASS/SMR was a one inch break in the cold leg followed by an emergency trip of the reactor and subsequent high pressure injection system activation. Since the LOFT facility was designed for traditional PWRs, it has a traditional U-tube steam generator, but TASS/SMR was written specifically for systems with helical steam generators, so a generic heat sink was used instead of an actual steam generator model. The data for both the steady state operations and the transient SBLOCA agree well with the TASS/SMR calculation. As mentioned in the previous tests, the code was found to calculate the primary side pressure lower than the measured pressure. As a result, the total flow through the break was miscalculated slightly but not by a significant amount. [17]

Once TASS/SMR was validated, it was then used to analyze accident scenarios in the SMART reactor. Many scenarios are required to be tested to prove that a reactor is, in fact, safe to build. Two of the main scenarios for the SMART reactor are the Steam Generator Tube Rupture (SGTR) [1] and the Small Break Loss of Coolant Accident (SBLOCA) [17].

To truly prove a reactor's ability to handle an accident, the worst case scenario must be analyzed. When modeling an SGTR, the limiting case was found to be a double-ended break low in a steam generator cassette where it was assumed nothing tripped the reactor until the operator initiated a SCRAM 30 minutes after

the initial break. The other conditions considered to be the most conservative case are as flows: high core power, low primary coolant temperature, high pressurizer pressure, low primary coolant flow rate, high pressurizer level, and a bottom skewed axial power shape. With all of these conditions, the most limiting case was modeled in TASS/SMR. Upon initiation of the event, the scenario was modeled such that it took 30 minutes for the operator to initiate the trip signal, another 5 seconds for the passive residual heat removal system isolation valves to open, and another 15 seconds for the main steam and feed water isolation valves to close and prevent further leakage. The model predicted that 28 tons of liquid would be leaked into the secondary side during the transient, but none of that was released to the atmosphere. As part of the SMART, design all secondary fluids are contained and the passive residual heat removal system has a high enough maximum pressure to prevent any vents into the atmosphere.

The SBLOCA model for the SMART reactor was built very similarly to the SGTR model except that the break was in the downcomer of the reactor vessel. Again, the limiting case was used, and the vessel was allowed to drain until a pressure trip caused the core to SCRAM and coolant to be injected. They found that the pressure drained quickly until the break was uncovered, and then it took several hours for the pressure trip to be reached. All the while, the core was never uncovered, and the cladding temperature never increased above its safety level. [17]

Through these tests and many others, TASS/SMR has been validated and then used to analyze the safety of the SMART reactor. In 2012, this analysis helped SMART to become the first SMR to ever be given Standard Design Approval [17]. This has proven both that TASS/SMR is a valid code for safety analysis and that SMRs in general are a valid technology for the future.

2.2.1 Steam Generator Correlations

The focus of this study is the correlations used in the steam generator model in TASS/SMR. Unlike other safety analysis codes TASS/SMR is designed for helical steam generators. Therefore, understanding those correlations and why they are used will helpful in understanding the analysis done in the Methods chapter. The steam generator model in TASS/SMR is broken into the internal and external flow correlations.

2.2.1.1 Internal Flow Correlations

TASS/SMR assumes that all flows inside the steam generator tubes are turbulent and, therefore, uses only turbulent heat transfer correlations. Starting in the sub-cooled liquid region, TASS/SMR uses Mori and Nakayama's correlation for turbulent liquids which is given in Equation 2.4. Once the flow reaches saturation though, another correlation must be used.

The developers of TASS/SMR decided to be creative when dealing with heat transfer correlation over the boiling region using a Modified Chen correlation. The Chen correlation, as was stated in an earlier section, was found to be accurate within 15% for heat transfer over the entire boiling range according to Owhadi et. al. [9]. The original Chen correlation [10] is as follows:

$$h = Sh_b + Fh_c \tag{2.6}$$

where h_b is a pool boiling heat transfer coefficient and h_c is a convective heat transfer coefficient. S and F are modifiers for each heat transfer coefficient known as the Suppression Factor and the Reynolds Factor, respectively. Chen gave descriptions for each factor but only solved for them graphically. In the original Chen corre-

lation, the pool boiling heat transfer coefficient is the Forster-Zuber correlation [18].

$$h_b = 0.00122 \left(\frac{k_f^{0.79} C_{pf}^{0.45} \rho_f^{0.49}}{\sigma^{0.5} \mu_f^{0.29} h_{fg}^{0.24} \rho_g^{0.24}} \right) \Delta T_{sat}^{0.24} \Delta P_{sat}^{0.75} \tag{2.7}$$

The convective heat transfer coefficient is the Dittus-Boelter equation.

$$h_c = 0.023 Re^{0.8} Pr^{0.4} \quad \frac{k}{D} \tag{2.8}$$

Since Chen did not give specific equations for the Suppression and Reynolds factors, Bjornard and Griffith [19] found curve fits for each. The Reynolds Factor is calculated using the turbulent Lockhart-Martinelli Parameter (χ_{tt}) which is primarily used in determining the two-phase pressure drop across a system where both phases are turbulent [20].

$$\chi_{tt}^{-1} = \quad \frac{x}{1-x}^{0.9} \quad \frac{\rho_f}{\rho_g}^{0.5} \quad \frac{\mu_g}{\mu_f}^{0.1} \tag{2.9}$$

$$F = 2.35 \left(\chi_{tt}^{-1} + 2.13 \right)^{0.736} \tag{2.10}$$

The Suppression Factor is calculated thus:

$$Re_{tp} = \frac{G\,(1-x)\,D}{\mu_f} F^{1.25} \left(10^{-4} \right) \tag{2.11}$$

$$S = \begin{cases} (1 + 0.12 Re_{tp})^{-1.14} & Re_{tp} < 32.5 \\ \left(1 + 0.42 Re_{tp}^{0.78} \right)^{-1} & 32.5 \leq Re_{tp} < 70 \\ 0.0797 & 70 \leq Re_{tp} \end{cases} \tag{2.12}$$

As mentioned previously, the developers of TASS/SMR modified the Chen correlation. This was done by replacing the convective heat transfer coefficient with a modified version of Seban and McLaughlin's correlation. This allows the convective term to account for the coiled geometry and make the overall correlation somewhat more accurate. The new version of Seban and McLaughlin's correlation is below and includes a quality term to strengthen its effect at low qualities.

$$h_c = 0.023 \quad \frac{k}{d_i} \quad (1-x)^{0.8} \, Re^{0.85} Pr^{0.4} \quad \frac{d_i}{D_c} \quad ^{0.1} \tag{2.13}$$

Once saturated vapor is reached in the steam generator using the Modified Chen correlation, then the gas version of Mori and Nakayama's correlation finishes out the calculation through the rest of the steam generator (Equation 2.4). That concludes the heat transfer coefficients inside of the tubes.

2.2.1.2 External Flow Correlation

The developers of TASS/SMR agreed with Kanevets and Politykina's finding that the Žukauskas correlation works on the outside of the tubes. Žukauskas did a significant amount of research and experimentation to develop his correlation. He started by analyzing flow over the surface of a cylinder. With experimental data, Žukauskas then looked at how the flow changed as it interacted with tubes in banks with different sized pitches between the tubes. He found that the first row of tubes acts like a normal cylinder in crossflow and that as the fluid passes the first several rows, the heat transfer gets higher because of the mixing caused by the tubes. The mean heat transfer in bank was found to follow Equation 2.5 which has two undefined coefficients. These coefficients, C and m, have been found experimentally by Žukauskas for staggered and aligned tube banks over a wide variety of Reynold's Number ranges. The list of these different coefficients can be found in most heat transfer textbooks [21].

Since the SMART reactor that TASS/SMR was built to model is a forced flow reactor, it is questionable whether the external flow models will work for a natural circulation reactor like NuScale's. The following chapter describes the facility where data was collected to test Žukauskas' correlation against the heat transfer coefficients of a helical coil steam generator in a natural circulation flow.

Chapter 3: MASLWR Facility Description

A good grasp of the MASLWR Test Facility's design and capabilities is essential when understanding the approach to solving for heat transfer coefficients in the steam generator. This section will first give an overview of the facility, paying close attention to the steam generator, and then a description of how tests are run and data is collected. Once a good understanding of the facility and its capabilities is reached, then an explanation of methods for calculating the heat transfer coefficient from the given data will be derived.

3.1 MASLWR Facility

As stated previously, the Multi-Application Small Light Water Reactor (MASLWR) Test Facility was built as a proof of concept for integrated reactors that use natural circulation as their mode of coolant movement. As such, it was not built with the thought of code validation and testing in mind, and the instrumentation of the facility is quite minimal in some sections. For privacy reasons, NuScale has asked that specific dimensions, other than those necessary for calculations, be excluded from this document as proprietary information. With this in mind, a description of the facility will be given, but only the steam generator section will be described in detail. Following that description, an outline of facility operations will be given to provide a better idea of how testing is conducted.

3.1.1 Primary System

The primary coolant system is housed inside of the Reactor Pressure Vessel (RPV). It is made of steel pipe, and it contains the core, chimney, pressurizer, steam generator (SG), and downcomer. The vessel and all of its components are rated for pressures and temperatures similar to those expected in a real nuclear power plant.

Primary circulation flow starts in the electrically heated core. It is made up of many cylindrical cartridge heaters arranged in a pattern similar to a nuclear core's fuel assemblies. The lower core plate and shroud around the core keep the fluid in close contact with the heater rods. The rod at the center does not provide any heating but is instrumented to measure temperature axially through the heated length of the core while several heater rods spread across the core have thermocouples at their center to give an estimate of rod centerline temperature and the radial temperature distribution.

After heating in the core and becoming less dense, the water flows upwards into the chimney which quickly necks down to a smaller flow area. Nearly halfway up the chimney, a cone-shaped obstruction laminarizes the flow and uses the pressure difference across the cone to calculate the flow rate using Bernoulli's Principle. At the end of the chimney, flow enters the upper plenum where it is redirected along the outside of the chimney to the steam generator.

The steam generator (SG) is situated in the annulus between the chimney's outer wall and the RPV vessel's inner wall. The dimensions of the section are given in Table 3.1. Inside of this section, fourteen helically shaped tubes wrap around the chimney several times before exiting through the vessel wall into a steam drum that is welded onto the outside of the RPV. The tubes are split into inner coils, middle coils, and outer coils. All coils in a particular group have the same dimensions that are listed in Table 3.2. Room temperature water enters the coils at the bottom and removes a large amount of energy from the primary coolant

by boiling and turning to superheated steam. This removal of energy causes the water in the primary side to cool and condense which adds to the flow's force in the downward direction. Instrumentation capturing the changes around the tubes is particularly sparse. Only six thermocouples, designated TF-701 through TF-706, measure the temperature vertically through the entire section. It is useful to note that when these thermocouples were being installed, one of the outer coils was punctured by the drill. That particular tube was filled with a sealant and has no influence on the calculations other than as a null volume in the primary side.

Table 3.1: MASLWR Steam Generator Section Dimensions

Component	**Dimensions**	**Units**
RPV Outer Diameter	14	inches
RPV Shell Thickness	1.25	inches
Chimney Outer Diameter	4.5	inches
SG Section Height	49.25	inches

Table 3.2: Steam Tube Dimensions

Bank	**Inner**	**Middle**	**Outer**
Direction	CW	CCW	CW
No. of Tubes	4	5	5
Tube Length	244.30in.	248.01in.	250.56in.
Coil Diameter	5.75in.	8in.	10.25in.
Rotations	13	9.5	7.5
Pitch	0.78	0.83	1.03
Rise/rotation	3.12	4.16	5.13
Total Coil Rise	40.5	39.5	38.5
Lead Length	6in.	6in.	6in.
Tube Outer Diameter	0.625in.	0.625in.	0.625in.
Tube Thickness	0.065in.	0.065in.	0.065in.

Once past the SG, the flow continues along the outside of the chimney and core in a region known as the downcomer. After passing the core, the flow is redirected in the lower plenum to flow back up through the lower core plate. The

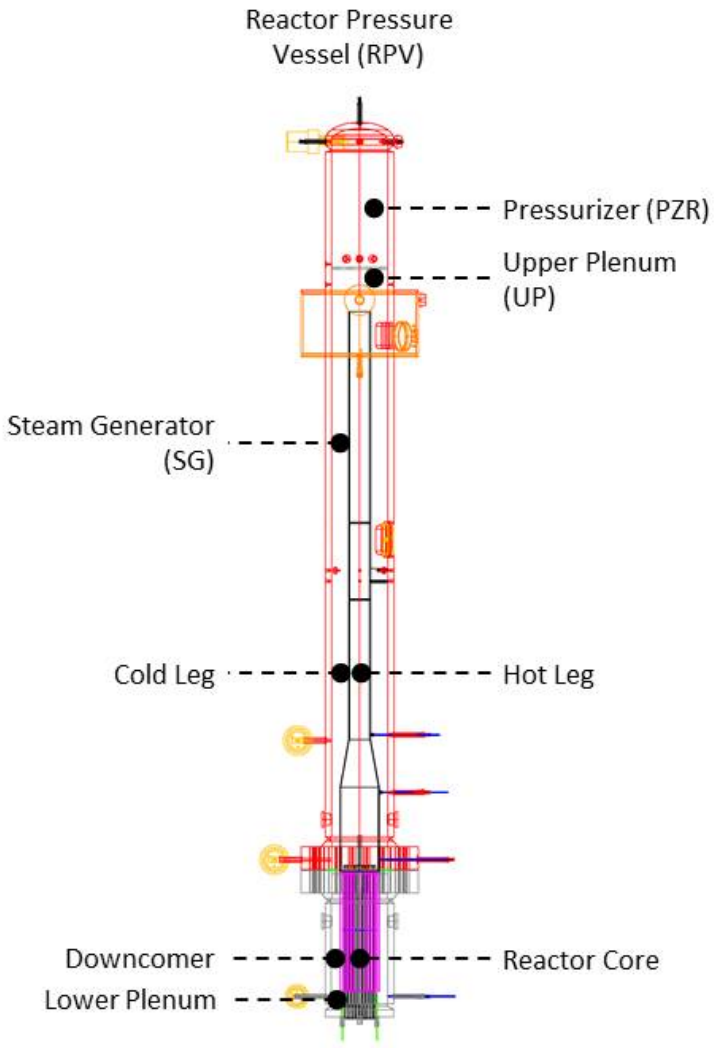

Figure 3.1: MASLWR Reactor Pressure Vessel Schematic

lower plenum is where the heater rods enter the vessel, but heat is only generated in the sections within the core.

Above the upper plenum mentioned earlier, is a region known as the Pressurizer (PZR). It maintains the primary system at a pressure that allows for the high temperatures required for testing without boiling in the core. The PZR is separated from the main circulation by a baffle plate that is essentially a steel plate with a few holes drilled in it. The baffle plate prevents the circulation flow from pulling too much heat from the pressurizer while still allowing for hydraulic pressure communication. A submerged heater operates to automatically keep the PZR at saturated steam temperatures well above the rest of the primary system's temperature. This maintains a steam bubble in the top few inches of the vessel which helps keep the system fairly stable because of the steam's inherent compressibility. If the vessel did not have a PZR section and was filled with solid water, the pressure would be very unstable and at such high temperatures, could easily over-pressurize the vessel and cause a leak that would, in turn, cause pressure to drop dramatically and allow the core to start boiling. With a steam bubble, the pressure can fluctuate and still be controlled without catastrophic ramifications.

3.1.2 Secondary System

The secondary system of the test facility provides the the water to the SG tubes and manages the steam flow after the water boils. City water is filtered and stored in a Feedwater Storage Tank (FWST) before entering either the primary or secondary systems. The FWST is kept above at least 50% to be sure that no air is entrained in the outlet lines and allowed to cause cavitation damage in the pumps. Two lines come off the outlet of the tank. One is known as the charging line, and it is used to fill the RPV if level is too low in the Pressurizer. The other line is known as the feedwater line, and it provides the water to the SG.

Figure 3.2: MASLWR Steam Generator Tubes Model

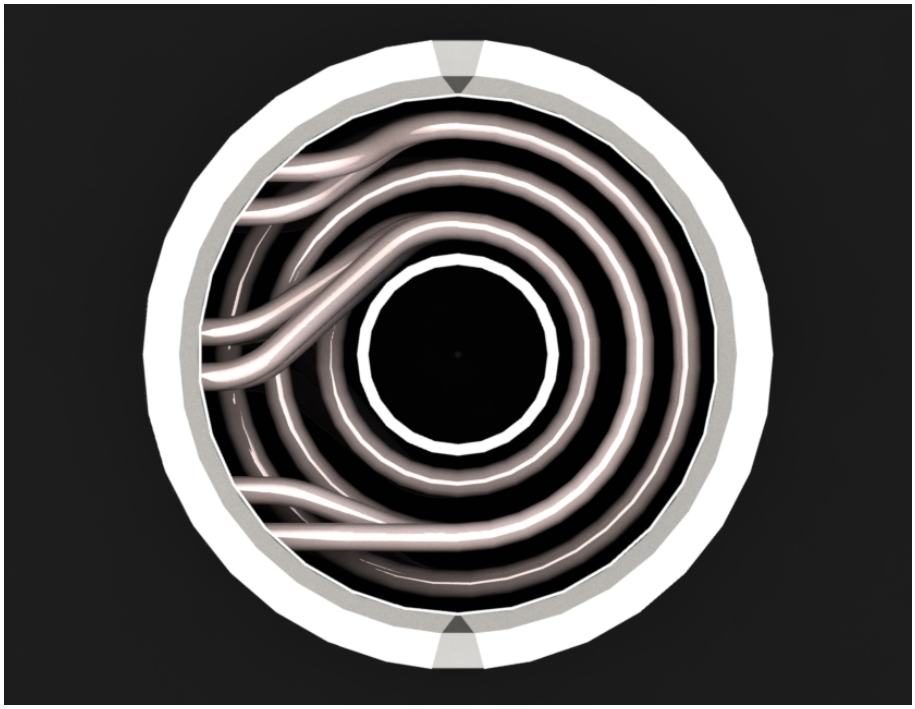

Figure 3.3: MASLWR Steam Generator, Top View

Water is pulled from the FWST by a pump known as the Main Feed Pump (MFP), and it passes a thermocouple, pressure transmitter, and flow meter to quantify the energy of the flow before it enters the SG. Once past the measuring devices, the flow splits into three streams; one for each set of coils. Each stream then passes through another flow meter and pressure transmitter before splitting into the individual SG tubes. The purpose of the second set of instrumentation is for the operator to distinguish any flow patterns or problems in the different coil groups. All of the steam tubes are made of 316 stainless steel pipe with an inner diameter of 0.495in. and a thickness of 0.065in. Once in the SG tubes, the water is superheated and dumped into the steam drum.

The steam drum collects all of the steam and directs it to an outlet line with a variable position valve that acts as the pressure regulator for the system. The regulator valve restricts the steam flow to build pressure and releases it to atmosphere through the vent stack. Any water that condenses inside of the steam drum is allowed to flow out through a steam trap that allows liquid to flow but acts as a steam boundary.

3.1.3 Containment and Cooling Pool Vessels

The other two vessels in the MASLWR facility are the containment and cooling pool vessels (CPV). Prior to the current test program the containment vessel was known as the high pressure containment vessel, or HPC for short. The HPC is connected by two upper and two lower automatic depressurization system (ADS) lines. The upper ADS lines are controlled by air actuated valves and are used to simulate steam flow during an accident scenario when a blowdown is initiated. The flow must pass through a scaled orifice before entering the HPC. Once a blowdown has condensed enough water, the lower ADS lines can be opened to allow the liquid water to flow back into the RPV and create a cooling loop. This is used to

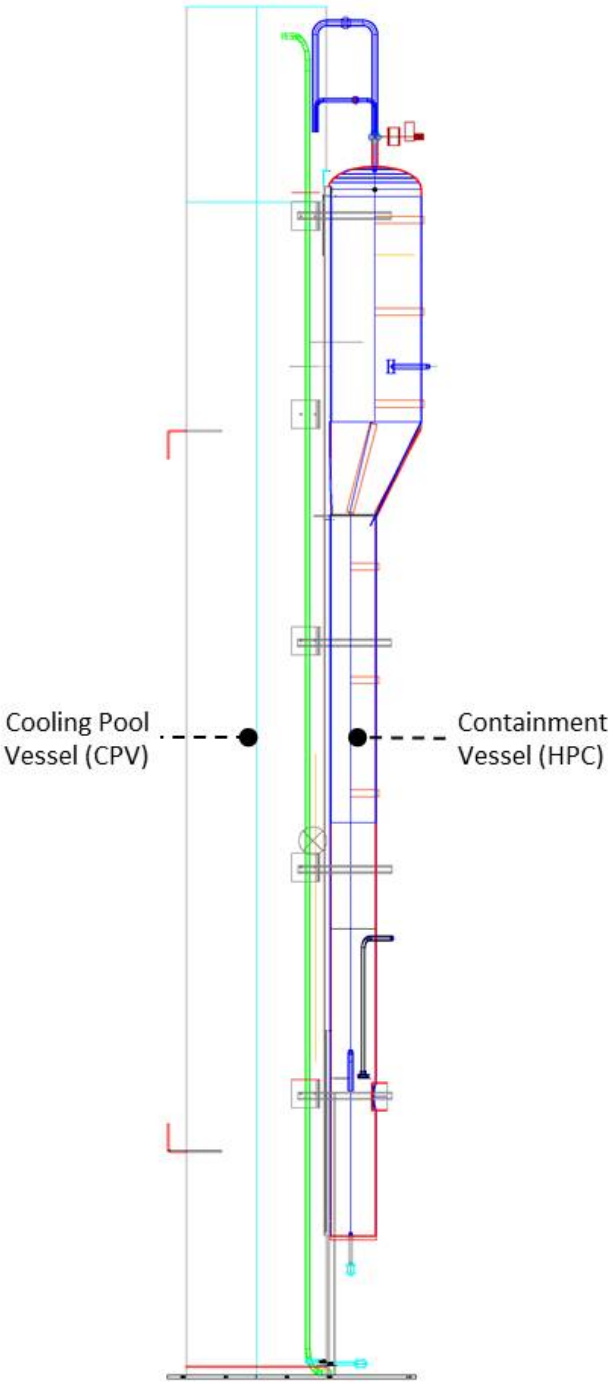

Figure 3.4: MASLWR Containment and Cooling Pool Vessels Schematic

demonstrate the facility's ability to perform long term cooling without the use of pumps that can fail in accident scenarios.

The HPC vessel is scaled in such a way that it has a large volume but requires a small heat transfer area to the CPV. This is because when scaled down, the heat transfer area, a length squared value, reduces more than volume, a length cubed value. The target area for heat transfer and steam condensation is known as the heat transfer plate (HTP), and it is instrumented with thermocouples to try to evaluate the heat transfer from the HPC to the CPV. The CPV is a large tank that is open to the atmosphere and filled with room temperature water. Both vessels have drain and fill valves to allow them to be drained for maintenance or filled to different levels for testing.

Table 3.3: Steam Generator Instrumentation

Instrument	**Units**	**Description**
TF-111	Fahrenheit	Upper Plenum Temp, Near Baffle Plate
TF-131,133,134	Fahrenheit	Primary Side Temp Below SG
TF-501	Fahrenheit	SG Inlet Temp
TF-611 - TF-634	Fahrenheit	SG Outlet Temps
TF-701	Fahrenheit	Primary Side Temp
TF-702	Fahrenheit	Primary Side Temp
TF-703	Fahrenheit	Primary Side Temp
TF-704	Fahrenheit	Primary Side Temp
TF-705	Fahrenheit	Primary Side Temp
TF-706	Fahrenheit	Primary Side Temp
FDP-131	$"H_2O$	Primary Side Flow Rate, Converted to lb_m/sec
FCM-511	lb_m/min	Outer Coils Flow Rate
FCM-521	lb_m/min	Middle Coils Flow Rate
FCM-531	lb_m/min	Inner Coils Flow Rate
PT-301	psig	Primary Side Pressure
PT-602	psig	Secondary Side Pressure

3.2 Data Collection

The MASLWR Facility is controlled by the Data Acquisition and Control System (DACS). This computer system controls the operations of the facility in addition to providing a quality path for the data to be recorded. All the instruments in the facility are calibrated and then the entire line from the instrument to the DACS records is checked to ensure that the data is accurate. The data is recorded once every second even though the DACS receives the data at a much higher rate. For the purposes of this analysis, the data used is averaged over several minutes to try and mitigate error from minor instrument fluctuations. When banks of instruments are used, like the thermocouples at the exit of the steam tubes, they are also averaged together to standardize the steam tubes.

3.3 Synopsis of Testing

When a test is run in the MASLWR Facility, very strict operational protocols are followed to heat up the plant and reach steady state before the test is initiated. These steps are written as Operating Instructions and Procedures. All test engineers are trained in these procedures and know them intimately. The first step to any test is an inspection of the facility and a valve lineup to put the facility in its standard test configuration.

Once the facility is lined up and has passed inspection, pressurization begins. This is accomplished by engaging the PZR heaters and allowing steam to vent all of the air out through the top of the RPV. After steam is observed venting, the facility is sealed and the PZR is allowed to pressurize the vessel to 250psig. When the RPV reaches 250psig, it is inspected for leaks. This allows operators to catch leaky valves and joints before they become a problem at high temperatures and pressures. Once the check is finished, the PZR is reengaged and set to reach

1250psig. As the vessel pressurizes further, the core and MFP are engaged to begin heating the rest of the primary system and to initiate natural circulation.

While heating, the core is limited to 25% power to prevent exceeding the maximum heat up rate for the facility. Over several hours, the RPV is heated and pressurized until the outlet temperature of the core is approximately 530F, and the vessel pressure is 1250psig. As the RPV heats up, the secondary system continually removes heat to preserve natural circulation. Once the RPV reaches at least 400F, the secondary side pressure is raised up to 150-300psig to increase the efficiency of the SG. For the observed test, the secondary pressure was 180psig. Once all of the set points are reached, steady-state must be found at the power level specified in the test. This is done by manipulating the secondary system flow rate until core outlet temperature, secondary flow rate, and both systems' pressures are steady at their set points.

At this point, the real test can begin. The observed test was meant to find steady-state at multiple power levels and to collect ten minutes of steady data to characterize the losses in the system. It has been observed in all tests done at the MASLWR Facility that steady-state is very difficult to achieve and is never completely steady. This is most likely because of the oscillatory nature of the competing flow and pressure controllers on the secondary system, but it also may come from the inherent instability of the primary loop.

Once testing is completed, the facility is usually shutdown by doing a blowdown through the upper ADS lines and performing a forced cooldown. A blowdown vents all of the pressure in the RPV into the HPC through the orifices in the upper ADS lines. Since the orifices are very small, the HPC never over pressurizes, and most of the steam condenses on the HTP. After both vessels reach a low enough pressure, the HPC can be vented to atmosphere through the vent stack. The forced cooldown then begins by using the charging pump to force cool water through the RPV and into the HPC. Once both vessels are below 200F, the facility can be locked down and the test day completed.

Chapter 4: Methods

This section is meant to describe the different approaches used to quantify the heat transfer coefficient on the outside of the helical steam generator tubes of the MASLWR test facility. To be able to accurately compare the Žukauskas correlation and the data from the MASLWR Facility, an extensive amount of data analysis and manipulation must be done. First, an overview calculation will be done to compare the heat transfer coefficients on a global scale using just the inlet and outlet information from both the primary and secondary systems. Then, a more comprehensive analysis will be done by discretizing the systems at the thermocouple levels to try and better grasp the trend of the heat transfer.

4.1 Global Analysis

A simple, global heat transfer calculation is performed by solving Newton's Law of Cooling (Equation 4.1) for the heat transfer coefficient (HTC) by using approximations for fluid temperature, wall temperature, and heat flux. [21]

$$q'' = h\Delta T = h\left(T_f - T_w\right) \tag{4.1}$$

The total heat transfer in the MASLWR SG was found by solving for the difference in enthalpy from the inlet of the steam tubes to their exit in the steam drum and multiplying it by the mass flow rate into the SG. The measurements for this calculation were taken from the secondary side to be sure that only the energy making steam is included. Dividing this total heat transfer ($\dot{Q}$) by the surface area of the outside of the tubes then results in the heat flux (q''). The total heat

transfer area on the outside of the tubes was calculated by multiplying the outer circumference of a single tube by the combined length of all the usable tubes in the SG.

Once the heat flux is known, then approximations for temperatures must be made. The temperatures at the inlet and the outlet of the primary side SG region were measured by TF-111 and the TF-130s respectively (Table 3.3). The fluid temperature was approximated by taking the arithmetic mean of the inlet and outlet. For a global analysis, there is no accurate way to calculate the wall temperature, so a guess was made by averaging the inlets of both the primary and secondary sides. With these two temperatures Equation 4.1 was solved for the HTC.

Many textbooks argue that a better way to approximate the HTC is to use a Log-Mean Temperature Difference (ΔT_{lm}) in Newton's Law of Cooling. This was calculated by using the inlet, outlet, and wall temperatures in the following equation. [21]

$$\Delta T_{lm} = \frac{(T_w - T_o) - (T_w - T_i)}{\ln \frac{T_w - T_i}{T_w - T_o}} \tag{4.2}$$

With ΔT_{lm} substituted into Equation 4.1, an improved HTC was calculated, and a more accurate comparison was made to Žukauskas' correlation.

4.2 Discretized Analysis

With the global calculations completed, a more detailed study was undertaken to calculate the tube wall temperature distribution across the length of the SG and to find the local heat transfer coefficients. It cannot be stressed enough that the instrumentation around the SG is too inadequate to compute a local HTC with accuracy. There is simply not enough information. This method is purely

an approximation using first principles to get an idea of what the HTC may be on the outside of the steam tubes. It also provides a better approximation to the average wall temperature that can be used to improve the global analysis. To begin, an explanation of the volume-discretization of the SG will be given. Then the calculations and methodology used to reach an HTC solution will be described in great detail. Assumptions and geometry values used in the calculations will be detailed along the way.

4.2.1 Discretization

Before any temperature or heat transfer calculations are be done, a lumped parameter analysis requires that the SG be to split into smaller sections. Since the only information measured directly in the SG region is by thermocouples, the heights of these instruments were used to delineate the edges of the numerical cells. Only six cells were able to be created between the following seven thermocouple positions: TF-131, TF-701, TF-702, TF-703, TF-704, TF-705, and TF-706. Early in the analysis, it was hoped that a seventh cell could be used between TF-706 and TF-111, but it was found to be too far away from the SG to reflect the primary side inlet temperature. Table 4.1 gives a better understanding of the size of the cells.

It is noticeable that the height of TF-706 is almost 14 inches below the top of the coil section of the RPV. This precipitates the first large assumption used in this analysis: that the section of the SG tubes above TF-706 has effectively no heat transfer. This assumption is required because there is no way to measure or calculate the temperature at the inlet to the SG region. Hopefully, in the future, modifications will be made to add instrumentation there, but for this analysis, TF-706 must be considered the top of the SG in the primary side, and TF-131 must be considered the bottom. Since the upper region of the SG should have only superheated steam when the system is operated at steady state conditions,

Table 4.1: Steam Generator Heights

Location	**Height**
TF-131,133,134	87.69in.
Bottom of Coil Section	89.69in.
TF-701	91.00in.
TF-702	98.125in.
TF-703	104.50in.
TF-704	111.125in.
TF-705	118.125in.
TF-706	125.25in.
Top of Coil Section	138.94in.
TF-111	145.44in.

then it is plausible to say that this assumption is valid because the heat transfer will be very low in that region.

With the primary side divided into six cells based on the heights of the surrounding thermocouples, the secondary side must also be divided along similar lines. Unfortunately, there are no thermocouples or other instrumentation inside the coiled tubes to aid in their division. It was decided that the division would be by proportional heights in the primary side. An average total length of an SG tubes was calculated to be 247.65in. This does not fall under the assumption stated above because the full volume and length of the SG tubes was used in the secondary side for this analysis. The proportional lengths are given in Table 4.2.

Table 4.2: Steam Generator Tube Cell Lengths

Cell Edge	**Height**	**Cell Number**	**Length**
1	0.00in.	1	21.82in.
2	21.82in.	2	46.98
3	68.80in.	3	42.03
4	110.84in.	4	43.68
5	154.52in.	5	46.15
6	200.67in.	6	46.98
7	247.65in.		

Within two of these cells, transitions will occur. First, a transition from single-phase liquid to two-phase boiling take place and then, a transition from two-phase boiling to single-phase steam. These transitions will split those particular cells and create even smaller cells. The determination of the location of the transition and its splitting will be detailed later in this study. With both volumes, the primary and secondary side, discretized into the smallest cells allowed by the facility's instrumentation, the description of the HTC calculations can be given.

4.2.2 Calculations & Methodology

The first part of any rigorous calculation is the preparation. By solving for much used constants that will be needed throughout the calculation at the beginning, time will be saved when coding the rest of the problem. The required pre-calculation constants are given in Table 4.3.

Table 4.3: Pre-Calculation Constants

Symbol	**Description**
ΔT_1	Temperature Difference Across Primary Side Cells
$T_{1,avg}$	Mean Temp in each Cell
c_{p1}	Specific Heat in Primary Side Cells
Δh_1	Enthalpy Change Across Primary side
Δh_2	Enthalpy Change Across Secondary side
$\Delta \dot{Q}$	Energy Balance Between Primary & Secondary
T_{sat}	Saturation Temperature of the Secondary Side
h_g	Saturated Vapor Enthalpy
Δh_{fg}	Enthalpy of Vaporization

When all the pre-calculations are finished, the next step is to solve for the bulk fluid temperatures inside of the SG tubes. To do this, the Conservation of Energy (CoE) equations were solved for the secondary side energy term. The CoE equations come in all forms depending on the assumptions made to reduce them. A generic form of the CoE can be seen in Equation 4.3. [22]

$$\rho c_p \frac{DT}{Dt} = \nabla \cdot k\nabla T - \nabla \cdot \overrightarrow{q}''_r + q''' + \beta T \frac{Dp}{Dt} + \phi \tag{4.3}$$

Where $\rho c_p \frac{DT}{Dt}$ is the substantive derivative of temperature, $\nabla \cdot k\nabla T$ is the diffusion term, $-\nabla \cdot \overrightarrow{q}''_r$ is the advective term, q''' is the volumetric heat generation term, $\beta T \frac{Dp}{Dt}$ is the pressure drop term, and ϕ is the friction term. To simplify this to a usable equation, some assumptions need to be made.

1. Flow is incompressible
2. Pressure is constant
3. There is no internal heat generation
4. Primarily an advective flow
5. Steady state
6. One-dimensional (only in vertical direction)

Assumptions 1, 2, and 6 are made to simplify the analysis while 3, 4, and 5 are required per the problem definition. With those assumptions made, the generic CoE becomes fairly simple and, more importantly, solvable with the known information.

4.2.2.1 Single-Phase Liquid

The CoE given in Equation 4.3 was for a single-phase liquid characteristic of the entire primary side and for the first part of the secondary side. Simplified for the assumptions stated above, it becomes:

$$\dot{m} c_p \frac{\partial T}{\partial z} = -q'' \xi_w \tag{4.4}$$

All that is left is the difference in energy from the inlet to the outlet and the advective heat transfer term. It was originally assumed that this was sufficient to characterize both the primary and early secondary side energy balances, but when the original calculation was completed, the energy balance appeared incorrect. Upon inspection, a substantial energy discrepancy was found. In the pre-calculations, the energy rate balance, $\Delta\dot{Q}$, was supposed to be near zero, but it was not. This is because the heat transfer from the chimney to the SG region was not accounted for. To correct for this, another term was added to CoE for the primary side.

$$\dot{m}c_p\frac{\partial T}{\partial z} + Q_z = -q''\xi_w \tag{4.5}$$

Q_z is defined by assuming that the linear heat rate across the chimney decreases linearly from the bottom to zero at the top. This is assumed because the larger amount of heat transfer through the chimney will logically be at the bottom of the SG where the water is cooler. By setting the total energy transferred to the SG region through the chimney equal to $\Delta\dot{Q}$ and defining the linear heat rate, q', as a line that, when integrated over the total height, equals $\Delta\dot{Q}$ an equation for Q_z can be generated. Figure 4.1 shows it a little better. The linear heat rate is defined as:

$$z_0 = \frac{2\Delta\dot{Q}}{H_{1,tot}} \tag{4.6}$$

$$q' = \frac{-z_0}{H_{1,tot}}z + z_0 \tag{4.7}$$

$H_{1,tot}$ is the total height of the primary side used in the calculation; for this analysis, it is from TF-131 to TF-706. Since Q_z is only the linear heat rate in a single cell, it is necessary to integrate q' across single cell with a height of ΔH to find the total heat transfer in that cell.

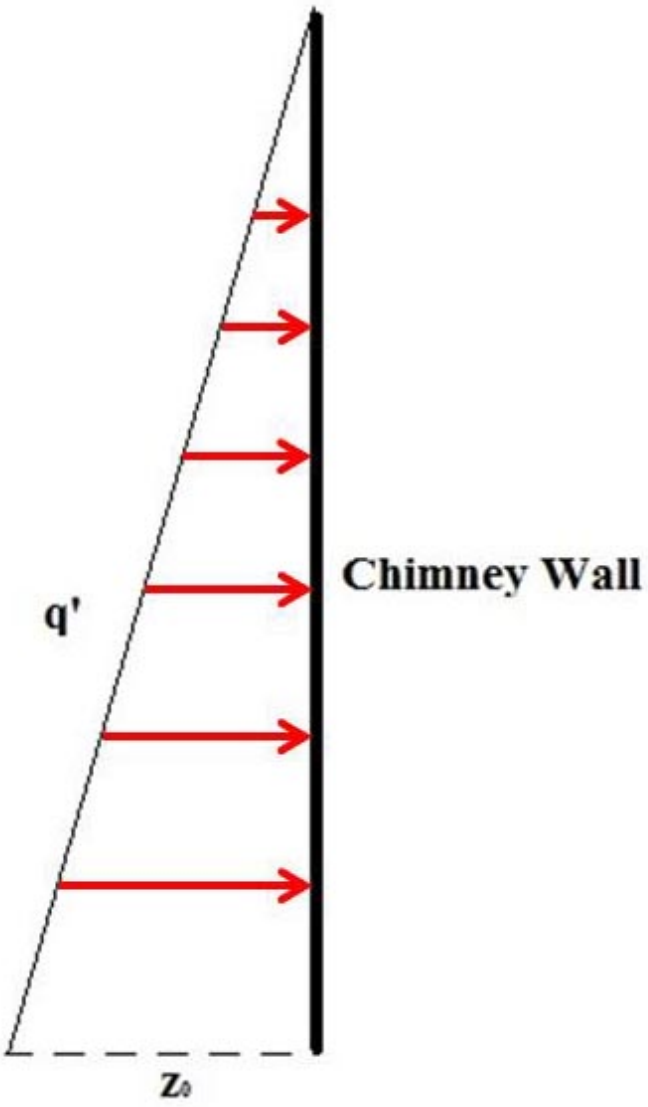

Figure 4.1: Linear Heat Rate Through Chimney Wall

$$\dot{Q} = \frac{-z_0}{H_{1,tot}} \int_{H_i}^{H_{i+1}} z dz + \int_{H_i}^{H_{i+1}} z_0 dz$$

$$\dot{Q} = \frac{-z_0}{H_{1,tot}} \frac{z^2}{2}\Big|_{H_i}^{H_{i+1}} + z_0 z|_{H_i}^{H_{i+1}}$$

$$\dot{Q} = \frac{-z_0}{2H_{1,tot}} \left(H_{i+1}^2 - H_i^2 \right) + z_0 \left(H_{i+1} - H_i \right) \tag{4.8}$$

To solve for Q_z, all that remains is to divide out an $(H_2 - H_1)$, or Δz, as it is referred to later on. Returning now to the CoE equations, they must be integrated over a single cell as well before they can be solved. When integrated, both single-phase CoE equations equal $\dot{Q}$. It should be noted that the Δz is returned to the Q_z when it is integrated. The primary side equation can then be integrated like so:

$$\dot{m}_1 c_{p,1} \int_z \frac{\partial T_1}{\partial z} dz + \int_z Q_z dz = - \int_z q_1" \xi_{w,1}$$

$$\dot{m}_1 c_{p,1} \Delta T_1(z) + Q_z \Delta z = -q_1" \xi_{w,1} \Delta z = \dot{Q}_1 \tag{4.9}$$

The secondary side can be similarly integrated.

$$\dot{m}_2 c_{p,2} \int_z \frac{\partial T_2}{\partial z} dz = - \int_z q_2" \xi_{w,2}$$

$$\dot{m}_2 c_{p,2} \Delta T_2(z) = -q_2" \xi_{w,2} \Delta z = \dot{Q}_2 \tag{4.10}$$

By setting the energy transfer $(\dot{Q})$ in the primary side equal to that in the secondary side, an equation can be created to link the temperatures from one side to the other. With the information in the primary side, this equation can be used

to determine the bulk fluid temperatures on the inside of the SG tubes.

$$(\dot{m}c_p\Delta T(z) + Q_z\Delta z)_1 = (\dot{m}c_p\Delta T(z))_2 \tag{4.11}$$

Once the left-hand side is calculated, it equals a constant, $\dot{Q}_1$, that is specific to each given cell. With $\dot{Q}_1$, Equation 4.11 can be solved for the temperature difference across each secondary cell. Since the inlet temperature is measured by TF-501 before the water is split into all of the tubes, it can be used as the starting place to calculate the rest of the temperatures by adding each cell's ΔT to the previous temperature. Of course, all of these new temperatures are assuming that there is liquid water completely filling the SG tubes; this is not the case. To approximate the level where the liquid water transitions to two-phase boiling, a linear interpolation must be done over the cell in which the transition happens to find the secondary side height where the temperature reaches T_{sat}. From this point, a new CoE is needed to handle two-phase flow.

4.2.2.2 Two-Phase Boiling

During boiling, the bulk fluid temperature can be assumed to be constant at the saturation temperature. This is not always true because the steam phase will be hotter than the liquid phase, but since this is a lumped parameter analysis, the boiling can be treated as a homogeneous equilibrium mixture. [22] The two-phase CoE equation can be written as:

$$\dot{m}\frac{\partial h_m}{\partial z} = -q"\xi_w \tag{4.12}$$

where h_m is the mixture enthalpy which is given by the quality of the steam, and the saturated vapor and steam enthalpies.

$$h_m = xh_g + (1-x)\,h_f = x\Delta h_{fg} + h_f \tag{4.13}$$

Since Δh_{fg} is constant for a given pressure, Equation 4.13 can be can be substituted into Equation 4.12. It then becomes:

$$\dot{m}\Delta h_{fg}\frac{\partial x}{\partial z} = -q"\xi_w \tag{4.14}$$

Like with the liquid CoE equation, the two-phase boiling equation must be integrated over the secondary cells as well.

$$\begin{aligned} \dot{m}\Delta h_{fg} \int_z \frac{\partial x}{\partial z}dz &= -\int_z q"\xi_w dz \\ \dot{m}\Delta h_{fg}\Delta x(z) &= -q"\xi_w \Delta z = \dot{Q} \end{aligned} \tag{4.15}$$

Now the mixture energy transfer can be set equal to the primary side's. This will allow the quality difference to be calculated for each cell.

$$\left(\dot{m}c_p\Delta T(z) + Q_z\Delta z\right)_1 = \left(\dot{m}\Delta h_{fg}\Delta x(z)\right)_2 \tag{4.16}$$

Since the primary side's heat transfer has already been solved for each cell, solving for the quality becomes a simple algebra problem. At the transition height, quality is set to zero. The quality gradient in the transition cell is then used to march the quality to the cell edge. With the cell edge quality calculated, the rest of the qualities can be advanced through the system by adding the next cell's Δx until a quality greater than 1.0 is seen.

When a quality is calculated to be over 1.0, then the previous cell must contain the second transition. Similar to the first transition cell, another linear interpo-

lation must be made to find the location where quality reached 1.0. Again, a new CoE equation is needed to continue the secondary bulk fluid temperature calculation into the single-phase steam region.

4.2.2.3 Single-Phase Steam

A similar energy equation to Equation 4.12 can be used to advance through the single-phase steam cells.

$$\dot{m}\frac{\partial h}{\partial z} = -q"\xi_w \tag{4.17}$$

By completing the same steps of integration, like Equation 4.15, and then setting the $\dot{Q}_2$ equal to that of the primary, a new equation can be written to solve for the enthalpy of the secondary side.

$$\left(\dot{m}c_p\Delta T(z) + Q_z\Delta z\right)_{Pri} = \left(\dot{m}\Delta h(z)\right)_{Sec} \tag{4.18}$$

Once Equation 4.18 is solved for the difference in enthalpy over each cell, it can be used to finish the temperature profile. The enthalpy at the next cell edge can be calculated by using the gradient of the enthalpy over the transition cell, multiplying it by the height difference from the transition location to the cell edge, and finally adding that to the saturated vapor enthalpy. Advancing through the final cells is a simple matter of adding the Δh to march through each cell. With the final enthalpies in place, temperatures can be found at all of their locations by using steam tables.

4.2.2.4 Fluid Temperature Correction

Now that a complete bulk fluid temperature profile has been calculated for the secondary side, the exit temperatures must be checked against those measured by the thermocouples in the steam drum. TF-611 through TF-615 measure the temperature at the exit of the outer coil tubes, TF-621 through TF-625 measure the temperature at the exit of the middle coil tubes, and TF-631 through TF-634 measure the temperature at the exit of the inner coil tubes. If the measured temperature differs from the calculated temperature, then a correction factor, F, will need to be added to the primary side heat transfer calculation, Equation 4.9.

$$\dot{m}c_p\Delta T(z) + Q_z\Delta z + F = -q"\xi_w\Delta z = \dot{Q} \tag{4.19}$$

The correction factor must be calculated to correctly adjust the total heat transfer across every cell such that the exit temperature is generated accurately. To do this, a root-finding method, such as the Bisection Method, can be used to converge the error to zero. The Bisection method requires two initial guesses of F, one high and one low, to allow the method to find the root. It was found through experimentation that guesses of -10 and 10 were sufficient to get errors below and above zero, respectively, for all cases used. With the guesses formulated, the next part of the method is to split the difference and calculate the error using a correction factor half way between the original guesses.

The next few steps are the heart of the Bisection Method. Depending on the sign of the new error at the half way point, the error must replace the original guess with the same sign. This is done to keep the root between the two guesses, but now the difference between the guesses has been halved. Now the process of halving the guess, calculating a new error, and replacing an error must be repeated until the error is below the set accuracy threshold. [23] For this analysis, the threshold

was set at 0.0001 to generate temperatures accurate to at least the thousandths place.

4.2.2.5 Wall Temperature Iteration

With the bulk fluid temperature calculated at all the cell edges, the next step is to calculate the temperature of the inside wall of the SG tubes. With this temperature, the temperature on the outside of the tubes can easily be calculated using Fourier's Law, and with the outside wall temperature, a heat transfer coefficient can be calculated. Before beginning these calculations, it makes them simpler if both of the transition cells are split into their separate regimes based on the transition heights calculated in the previous sections. This includes splitting the total heat transfer in the transition cells between the two new cells based on the cell's length ratio. A length ratio is the fraction of the new cell's length compared to the entire transition cell's length. Now there are eight cells and nine cell edges to work with.

After splitting the cells the heat flux into each cell must be calculated by dividing the total heat transfer rate by the combined wetted perimeter for all of the tubes and the length of each cell.

$$q'' = \frac{\dot{Q}}{\Delta z \xi_w} \tag{4.20}$$

Using this method, the heat flux is calculated to be the same over the split cells. This is inherently untrue, especially in the cells transitioning from boiling to steam flows. At that transition, the heat flux must decrease rapidly because superheated steam is an insulator and has very low heat transfer coefficients. Steam cannot handle that much heat flux with the given parameters of the system. If the heat flux is left unchanged in the transition cells, those cells will not be able to converge

to a solution in the iterative solver to be described later. A new method to weight the heat flux in the transition cells is needed before a solution can be found for the wall temperatures.

The solution is different depending on where the transition actually occurs and will change depending on the power level at which the facility is operating. At lower power levels, the transition happens in a cell before the last of the original six cells. In that case, the last cell's heat flux can be used for the steam portion of the transition. Since the total heat transfer over the entire original transition cell must be preserved, the new heat flux in the steam cell must be used to find the heat transfer rate and heat flux in the boiling cell. The following equations were used with subscripts to denote the steam and boiling cell values.

$$\begin{aligned} q''_{s,new} &= q''_{s+1} \\ \dot{Q}_{s,new} &= q''_{s,new} \Delta z \xi_w \\ \dot{Q}_{b,new} &= \dot{Q}_{tot} - \dot{Q}_{s,new} \\ q''_{b,new} &= \frac{\dot{Q}_{b,new}}{\Delta z \xi_w} \end{aligned} \tag{4.21}$$

If the transition occurs in the last of the original cells, like at the higher power levels, the same method cannot be applied. The solution for these cells is to use a similar weighting method as described for the heat transfer into the primary side from the chimney. Another large assumption must be made here and verified to be valid. The assumption is that the linear heat rate in the transition cell goes to zero at the exit. If the known steam outlet temperature is lower than the inlet to the SG region, then there must be some amount of linear heat rate at the exit of the tubes, but it should be very small because of the superheated steam in the tubes. At the end of this methodology, a description of the validation calculation will be made.

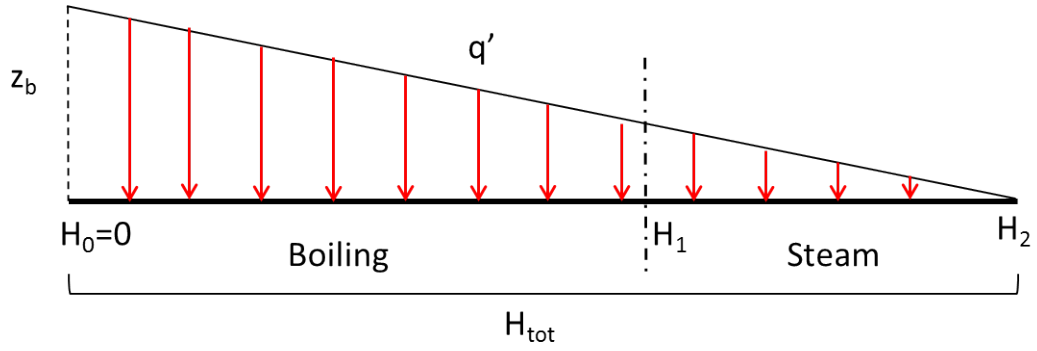

Figure 4.2: Transition Cell Heat Transfer Rate Redistribution

Similar to the calculation for the heat transfer rate in the chimney, all that is needed is to find the z_0 from Equation 4.7 and substitute it with the length of the cell into Equation 4.8. Figure 4.2 shows this in a more understandable way. With an updated heat transfer rate in either the boiling or steam cell, the other can be found by subtracting the updated $\dot{Q}$ from the original transition cell's heat transfer rate. All that is left is to convert those heat transfer rates to heat fluxes, and the the temperature iteration can begin.

Again, the Bisection Method will be used, but in a slightly different way. This time, a wall temperature will be guessed, and a heat transfer correlation used to find the error. The goal is to find wall temperatures that will satisfy Newton's Law of Cooling. Rewriting Equation 4.1 to solve for error looks like:

$$0 = q'' - h\left(T_w - T_f\right) \tag{4.22}$$

The calculation should step through each cell, first recognizing the regime (liquid, boiling, or steam) and then performing the iteration to solve for the wall temperature using the correction heat transfer correlation. Each of the correlations has been described in detail in the Literature Review chapter. In the liquid region, it was found that the flow was laminar because the Reynold's Number (Re) was less

than the critical Re, so the Schmidt correlation (Equation 2.3) was used instead of the Mori and Nakayama correlation. Re_{crit} was calculated using the Srinivasan et. al. [24] method.

$$Re_{crit} = 2100 \left[1 + 12 \left(\frac{d_i}{D} \right)^{0.5} \right] \tag{4.23}$$

The boiling region uses the Modified Chen Correlation (Equation 2.6) detailed in the description of the TASS/SMR code. Finally, the Mori & Nakayama correlation (Equation 2.4) for a gas was used for the superheated steam cells.

The initial guesses for the wall temperature are the bulk fluid temperature coming into that cell and the primary side fluid temperature from the other cell edge. These encompass the maximum and minimum logical values that the temperature could be. It should be noted that the wall temperature that is being solved for is an average for the entire cell and is, therefore, located at the center of the cell rather than the edges like previous temperatures. This also means that some fluid property values used in the heat transfer calculations should be averaged over the cell. These are fluid velocity and quality. Normally bulk fluid temperature would need to be averaged as well but since the flow is already assumed to have no heat diffusion, it is also assumed to behave as an upwind system, meaning that the temperature at the inlet cell edge can be used for the bulk fluid temperature.

Once all of the cells have converged to a wall temperature solution that makes logical sense, the heat must be conducted through the wall. Fourier's Law for hollow cylinders allows for the conduction through a pipe wall to be calculated. [21]

$$\dot{Q} = -\frac{2\pi L k \left(T_{1,w} - T_{2,w} \right)}{\ln \left(\frac{r_2}{r_1} \right)} \tag{4.24}$$

The thermal conductivity, k, can be approximated at the known wall temperature because its change through the pipe will be negligible. Since everything but the outer wall temperature is now known, algebra can be used to solve for it. With these outer wall temperatures completed, cells that were split for the transition calculations may be brought back together by multiplying them by their cell's length ratio and adding them together. This gives a length weighted average for the combined transition cell. Now Newton's Law of Cooling, Equation 4.1, can be used again to solve for the heat transfer coefficient.

$$h = \frac{\dot{Q}}{A\left(T_f - T_{1,w}\right)} \tag{4.25}$$

It should be remembered when computing this last part, that the area term will be a multiplication of the tube's outer perimeter and the length of each SG in the primary section. As discussed in the Discretization section, the primary SG region with usable measurements does not cover the entire SG, so the outer tube lengths must be scaled back to accommodate for it. It should also be noted that for this analysis, the primary side is also considered an upwind system, and therefore the fluid temperatures used are from the top edge of each cell. With the completion of Equation 4.25 for all six primary cells, the HTC has finally been found.

4.2.2.6 Assumption Validation

During the attempt to correctly weight the heat transfer rate in the boiling-to-steam transition cells, it was assumed that the linear heat rate in the transition cells that border the end of the SG tubes linearly decreased to zero. This only occurs in higher power level tests, and since it is not physical, a validation must be made to be sure that assumption's error is negligible. The process for this validation is circular, but it should give an indication as to whether the assumption

can be made or not. The validation test will be to calculate a new linear heat rate at the very exit of the SG tubes, redistribute the weighted heat transfer rate, and finally recalculate wall temperatures and heat transfer coefficients to see if they change significantly.

To first calculate the new linear heat rate at the very exit, a system of three equations may be solved by matrix inversion. The equations are the three separate heat transfer equations.

$$q' = 2\pi r_1 h_1 \left(T_f - T_{1,w}\right) \tag{4.26}$$

$$q' = \frac{2\pi k \left(T_{2,w} - T_{1,w}\right)}{\ln \frac{r_1}{r_2}} \tag{4.27}$$

$$q' = 2\pi r_2 h_2 \left(T_{2,w} - T_v\right) \tag{4.28}$$

Before these equations can be solved, though, some definitions must be made. Since the HTC correlations used in this analysis all require a wall temperature, one must be assumed in the correlations to prevent the system from having too many unknowns. This is done by averaging the inlet temperature at the top of the primary side and the outlet temperature at the top of the secondary side. The secondary side heat transfer coefficient, h_2, is still calculated using the Mori & Nakayama correlation turbulent gas with the fluid temperature at the SG tube outlet temperature.

The primary side HTC is a little more difficult to find. The only correlation available is the Žukauskas correlation that is being tested in this analysis. To give it some amount of accuracy for this validation, the Žukauskas correlation can be modified by using the HTC calculated for the last cell in the original analysis to solve for a new multiplication coefficient. With the coefficient, C, in the Žukauskas correlation replaced, a reasonable HTC can be calculated at the very top cell edge

and used as h_1. Now the only unknowns are the linear heat rate and the two wall temperatures. To solve for these unknowns, the system of equations can be made into a traditional matrix equation and solved.

$$\begin{bmatrix} 1 & 0 & \frac{1}{2\pi r_1 h_1} \\ \frac{2\pi k}{\ln\left(\frac{r_1}{r_2}\right)} & \frac{-2\pi k}{\ln\left(\frac{r_1}{r_2}\right)} & -1 \\ 0 & 1 & \frac{-1}{2\pi r_2 h_2} \end{bmatrix} \begin{bmatrix} T_{1,w} \\ T_{2,w} \\ q' \end{bmatrix} = \begin{bmatrix} T_f \\ 0 \\ T_v \end{bmatrix} \tag{4.29}$$

To solve this problem a matrix inversion can be done.

$$\begin{aligned} Ax &= b \\ x &= A^{-1}b \end{aligned} \tag{4.30}$$

Now that the new linear heat rate at the top cell edge has been calculated, the heat transfer rate must be redistributed between the two parts of the transition cell by finding a new slope for the linear heat rate that, when integrated, will still give the correct total heat transfer rate. This can be done by changing the triangular representative of the linear heat rate, q', in Figure 4.2 into a trapezoidal shape with a top height of z_t and similar base called z_b like in Figure 4.3. The top height is equal to the q' found in the matrix equation above. Using the top height and the total heat transfer rate in the transition cell, a base height can be found similar to Equation 4.6.

$$z_b = \frac{2\dot{Q}_{tot}}{H_{tot}} - z_t \tag{4.31}$$

Using the new base height, a new z_0 can be calculated and substituted into Equation 4.8.

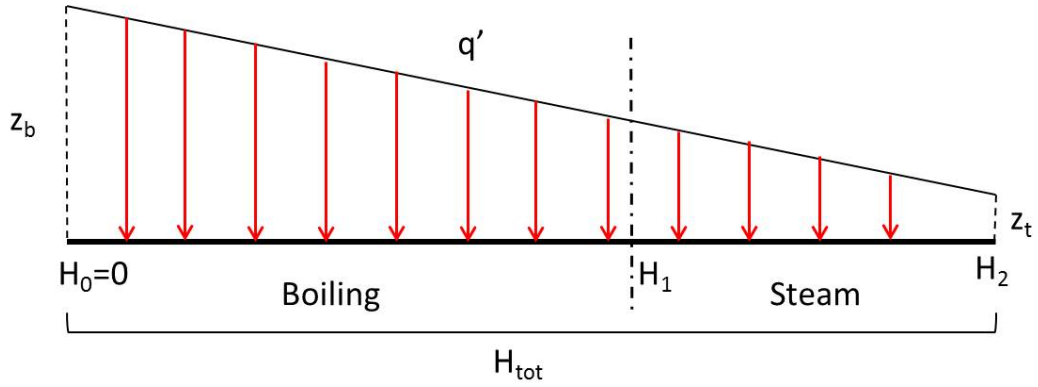

Figure 4.3: Transition Cell Heat Transfer Rate Redistribution

$$z_0 = z_b - z_t \tag{4.32}$$

$$\dot{Q} = z_0 \Delta H \quad 1 - \frac{H_{i+1} + H_i}{H_{tot}} \tag{4.33}$$

With a new heat transfer rate calculated for each part of the transition cell, new heat fluxes can also be generated. From here, the same methodology used for the original analysis can be used to solve for new wall temperatures and a new HTC in the final cell. A comparison of the changed heat fluxes, wall temperatures, and heat transfer coefficients will be given in the Results & Discussion chapter.

4.2.2.7 Final Calculations

To finish the calculations and methods described for the discretized analysis, the Žukauskas correlation must be used with the newly generated wall temperatures to generate heat transfer coefficients for comparison. The C and m coefficients in the correlation shall be taken to 0.27 and 0.63, respectively. These coefficients reflect the tube alignment and Reynold's Number range of the primary side [21].

4.3 Updated Global Analysis

A global analysis and a discretized analysis have both been described in detail above. As a conclusion to the analysis, a combination of the two can be done. Since wall temperatures were generated in the discretized analysis for all six cells, a length weighted average can be performed to provide a more accurate global wall temperature. This updated wall temperature can be used in both the standard temperature difference and the log-mean temperature difference calculations described in the first section of this chapter. These updated calculations may prove to be the most helpful of all the methods described in this chapter.

Chapter 5: Results & Discussion

The purpose of this section is to give the values that were used as inputs into the calculations described in the Methods chapter and to present the results of those calculations. The input values for the system shall be given first, and the results of both the global and discretized calculations shall be presented. Discussion and analysis of the results will be performed as they are presented. All calculations were performed in Microsoft Excel except for the discretized analysis which was computed using Matlab.

5.1 Calculation Inputs

Test data was taken from the OSU MASLWR RPV Flow Loss Characterization test, OSU-MASLWR-13008-R0, that was completed on April 2, 2013. Steady state was achieved seven different times as the facility power was cycled high to low and back to high. All measured values are averaged over the time spent in steady state.

Before detailing the results this study will outline the trends in the input data. At higher power levels, higher primary and secondary mass flow rates are required to remove the heat generated in the core. To maintain steady temperatures at the outlet of the core at high power levels, the temperature drop through the SG region must also be larger. This can be seen in Figure 5.1. It can be observed in the figure that the temperature trends suggest that boiling and steam dry-out occur much lower at low powers. This is seen by the sharp rise and then flattening of temperature. It can also be observed that the higher temperatures barely seem to reach the end of the boiling region before reaching the top of the SG.

Table 5.1: Calculated Volume Values From OSU MASLWR Test Facility

Average SG Tube Length	247.65in.
Tube Inner Wetted Perimeter	20.22in.
Tube Outer Wetted Perimeter	25.53in.
Primary Cross Flow Area Before Tubes	$87.96in.^2$
Primary Cross Flow Area in SG	$66.35in.^2$
Combined Cross Flow Area in Tubes	$2.50in.^2$

Table 5.2: Averaged Input Values From Test Data

Value	**392 kW**	**300 kW**	**200 kW**	**100 kW**
$\dot{m}_1$	$4.707 lb_m/s$	$4.148 lb_m/s$	$3.444 lb_m/s$	$2.386 lb_m/s$
$\dot{m}_2$	$17.93 lb_m/min$	$13.41 lb_m/min$	$8.860 lb_m/min$	$4.226 lb_m/min$
P_1	1250psig	1250psig	1250psig	1250psig
P_2	180psig	180psig	180psig	180psig

Value	**200 kW(2)**	**300 kW(2)**	**392 kW(2)**
$\dot{m}_1$	$3.457 lb_m/s$	$4.169 lb_m/s$	$4.700 lb_m/s$
$\dot{m}_2$	$9.021 lb_m/min$	$13.61 lb_m/min$	$17.94 lb_m/min$
P_1	1250psig	1250psig	1250psig
P_2	180psig	180psig	180psig

Table 5.3: Averaged Temperature Values From Test Data

Value	**392 kW**	**300 kW**	**200 kW**	**100 kW**
SG Tube Inlet	57.61^oF	57.62^oF	58.93^oF	61.90^oF
SG Tube Outlet	484.83^oF	514.05^oF	525.41^oF	525.83^oF
TF-13Xs	462.89^oF	473.69^oF	489.01^oF	502.95^oF
TF-701	468.75^oF	478.42^oF	490.38^oF	506.98^oF
TF-702	475.66^oF	485.74^oF	503.06^oF	512.52^oF
TF-703	482.34^oF	495.42^oF	514.15^oF	524.04^oF
TF-704	494.79^oF	513.70^oF	524.42^oF	524.87^oF
TF-705	514.65^oF	520.81^oF	525.80^oF	525.22^oF
TF-706	522.14^oF	523.89^oF	526.91^oF	525.97^oF

Value	**200 kW(2)**	**300 kW(2)**	**392 kW(2)**
SG Tube Inlet	60.26^oF	60.05^oF	59.03^oF
SG Tube Outlet	524.64^oF	514.30^oF	476.74^oF
TF-13Xs	487.94^oF	475.45^oF	463.70^oF
TF-701	489.49^oF	480.14^oF	469.57^oF
TF-702	501.65^oF	487.56^oF	476.69^oF
TF-703	512.11^oF	496.84^oF	483.59^oF
TF-704	523.71^oF	513.88^oF	495.15^oF
TF-705	525.27^oF	521.59^oF	511.82^oF
TF-706	526.37^oF	525.51^oF	522.17^oF

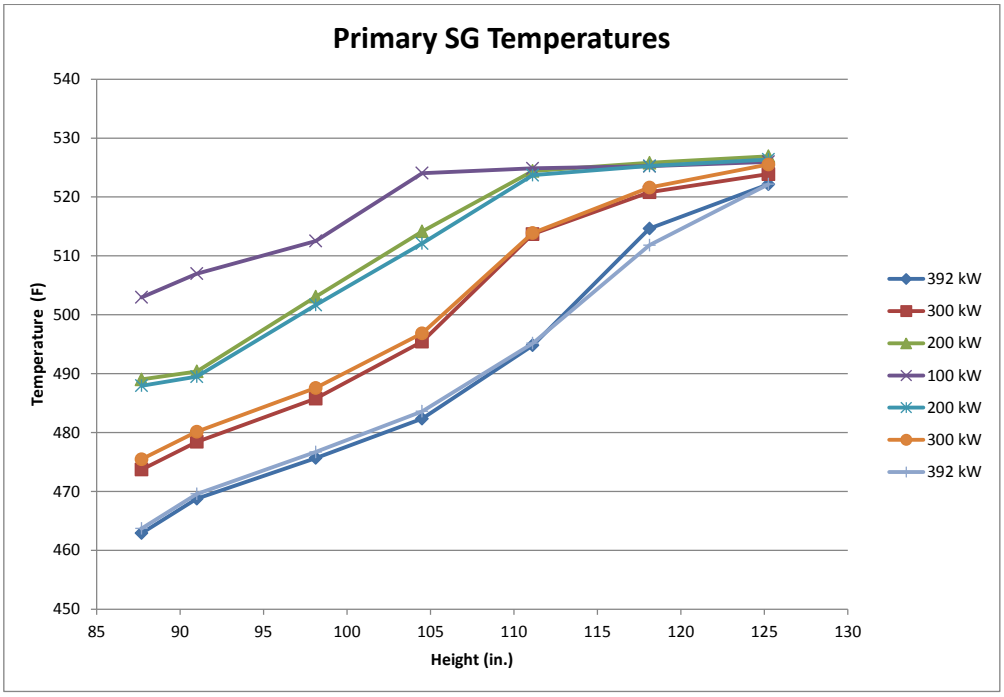

Figure 5.1: Primary Side Temperatures at Different Power Levels

5.2 Global Analysis

Global heat transfer coefficients were found using Equation 4.1, Newton's Law of Cooling. By taking the average primary fluid temperature, a guess for the average wall temperature, and the calculated total heat transfer rate, the initial HTCs were found. The standard temperature difference was used to calculate the first heat transfer coefficients across the different steady state conditions. Steady state was defined as ten minutes of data with less than 10F variance in the core outlet temperature. Each repeated power level is consistent enough to verify the repeatability of the steady-state conditions in the test. The solutions for the global heat transfer coefficients using the standard temperature difference are summarized in Table 5.4.

Table 5.4: Global Heat Transfer Coefficients Using Standard Temperature Differences Compared to the Žukauskas Correlation

Power	**Calculated HTC**	**Correlation HTC**
(kW)	(W/m^2C)	(W/m^2C)
392	849.3744	2074.192
300	626.6539	1919.737
200	402.0239	1717.466
100	186.5868	1367.995
200	411.0613	1721.439
300	635.9913	1930.853
392	846.8668	2074.298

The log-mean temperature difference approach to calculating the global heat transfer coefficients results in slightly larger HTCs. This is because the temperature difference calculated is slightly smaller when used in Newton's Law of Cooling. The log-mean temperature difference does not effect the lower power levels nearly as much because the change in the temperature difference is too small. The solutions for the global heat transfer coefficients using the log-mean temperature difference (Equation 4.2) are summarized in Table 5.5.

Table 5.5: Global Heat Transfer Coefficients Using Log-Mean Temperature Differences Compared to the Žukauskas Correlation

Power	**Calculated HTC**	**Correlation HTC**
(kW)	(W/m^2C)	(W/m^2C)
392	855.4905	2074.192
300	629.4985	1919.737
200	402.9495	1717.466
100	186.7257	1367.995
200	412.0398	1721.439
300	638.875	1930.853
392	852.8511	2074.298

For all of these analyses, the Žukauskas correlation was used to calculate an HTC using the same information. As described in the Literature Review chapter, the Žukauskas correlation was calculated by using Equation 2.5. The coefficients C and m are defined by the Reynold's number of the flow entering the tube bank. Since the Re is between 3000-6000 for all test cases, C equals 0.27, and m equals 0.63. [13]

Both sets of calculations differ greatly from the Žukauskas correlation's heat transfer coefficient. The general slope of the trends appear to be similar though. On average, both calculations are 1260 W/m^2C less than the HTC found by using the correlation. A significant portion of this difference stems from the inaccuracy of the wall temperature guess. The Updated Global Analysis section will describe this in more detail.

5.3 Discretized Analysis

The calculations described in the Methods chapter for the Discretized Analysis had three main evolutions: first, to find the bulk fluid temperatures in the secondary sides; then, to converge to an inner tube wall temperature; and finally, to conduct

the temperature through the tube wall and solve for the local heat transfer coefficients. The bulk fluid temperatures are calculated at the cell edges while the wall temperatures and HTCs are averaged over the cells. To begin, the bulk fluid temperatures are presented in Figure 5.2 through Figure 5.5.

The bulk fluid temperatures show what was hinted at in the discussion of the measured primary fluid temperatures. At higher power levels, and thus higher flow rates, the boiling region is shifted upward in the SG tubes. This is seen by the flat sections of graph at the saturation temperature covering higher cells in the higher power tests. The first and last temperatures are those measured in the facility. With seven temperature points calculated, the procedure for iteratively solving for the wall temperature was begun for each power level test.

Each wall temperature took 30-50 iterations to converge to their respective values. All of the distributions initially increase rapidly, then turn over and decrease before having another increase in the final cells. The initial increase makes sense, but the decrease can be a little confusing. This occurs because the heat transfer rate in the upper boiling region is so high that it actually cools the tube walls.

Unlike the bulk fluid temperatures, the wall temperatures do not always overlap well between tests at the same power level. This is caused by slight differences in the phase transition heights in each test. If the splits in the transition cells are even slightly different, the height has a large impact on the wall temperature because of the different weighting of the heat transfer rate in each part of the cell.

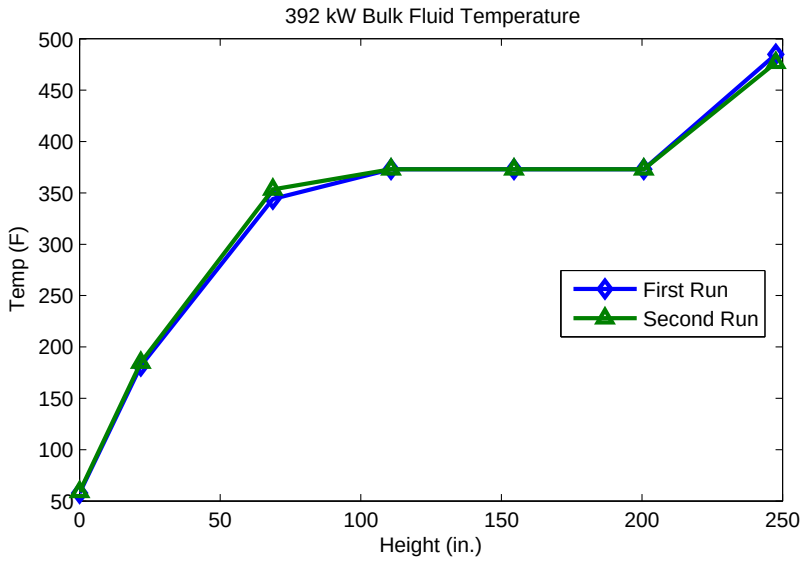

Figure 5.2: Secondary Bulk Fluid Temperature at 392 kW

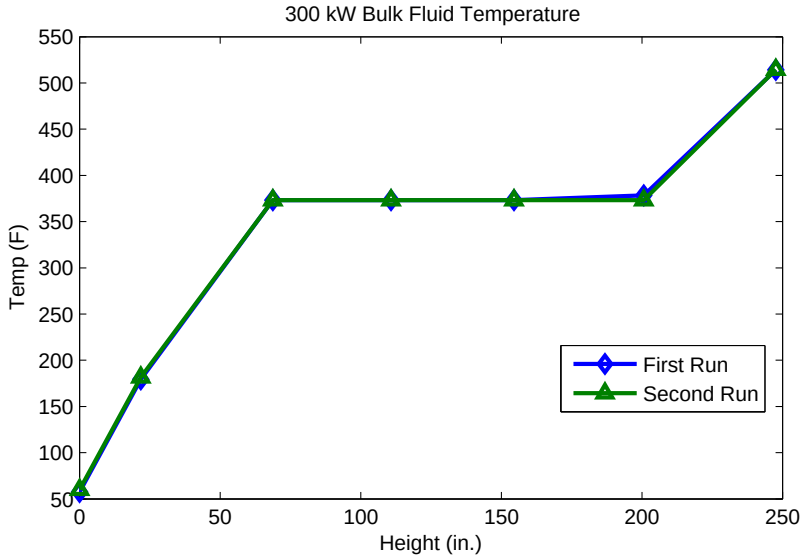

Figure 5.3: Secondary Bulk Fluid Temperature at 300 kW

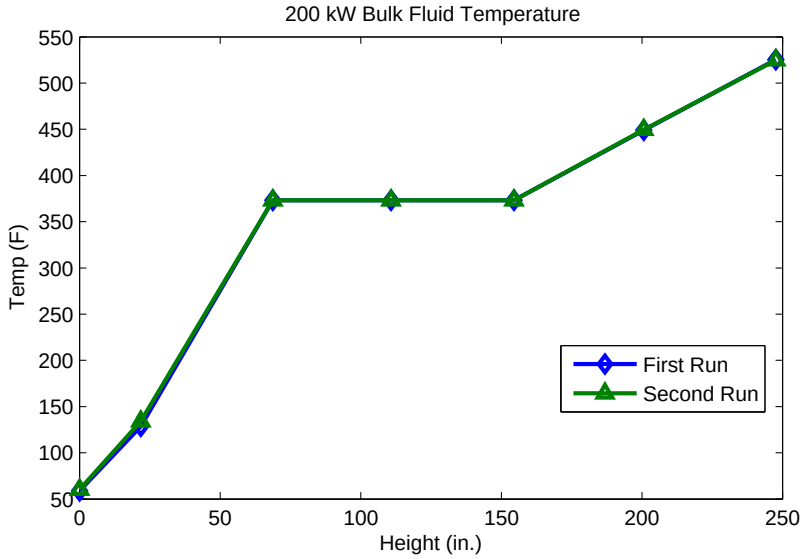

Figure 5.4: Secondary Bulk Fluid Temperature at 200 kW

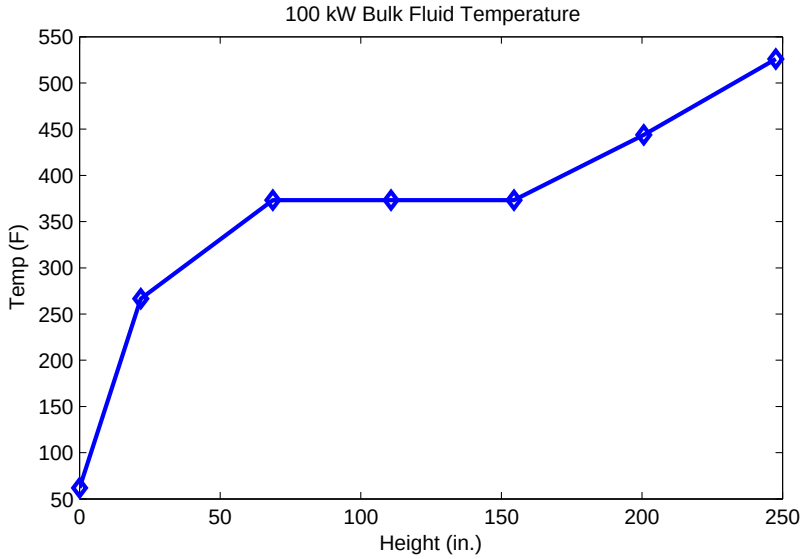

Figure 5.5: Secondary Bulk Fluid Temperature at 100 kW

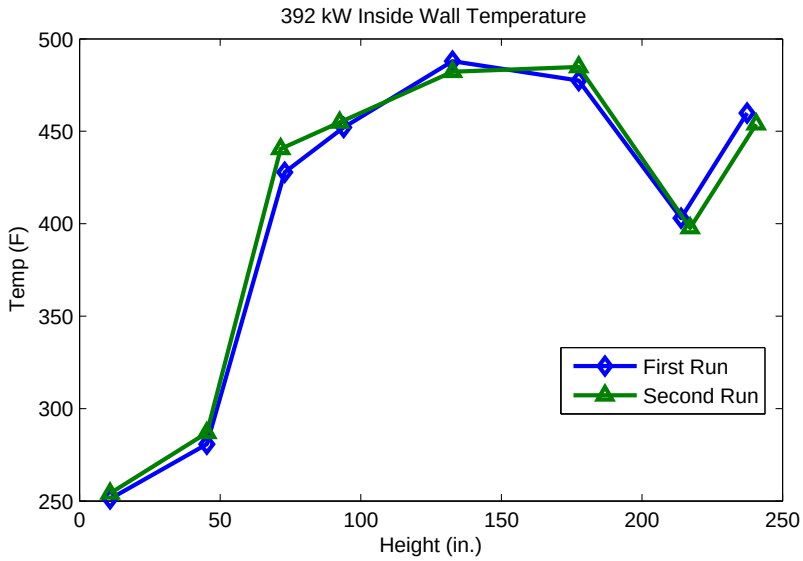

Figure 5.6: Inner Tube Wall Temperature at 392 kW

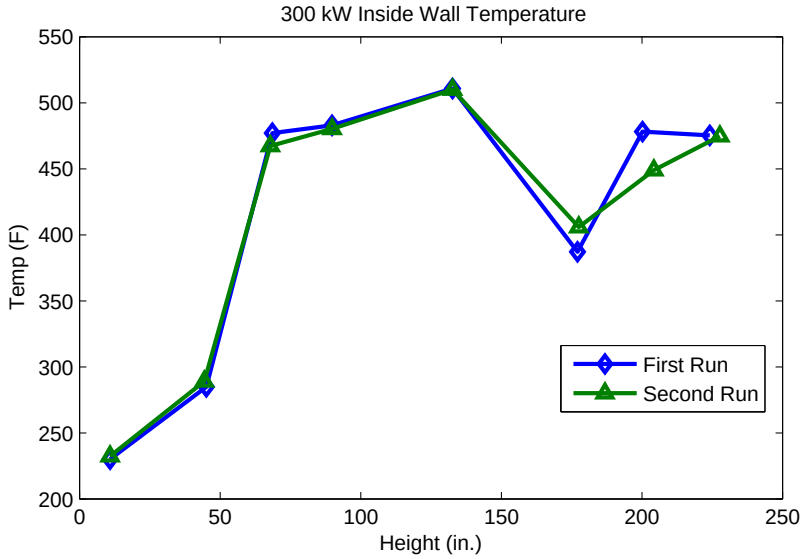

Figure 5.7: Inner Tube Wall Temperature at 300 kW

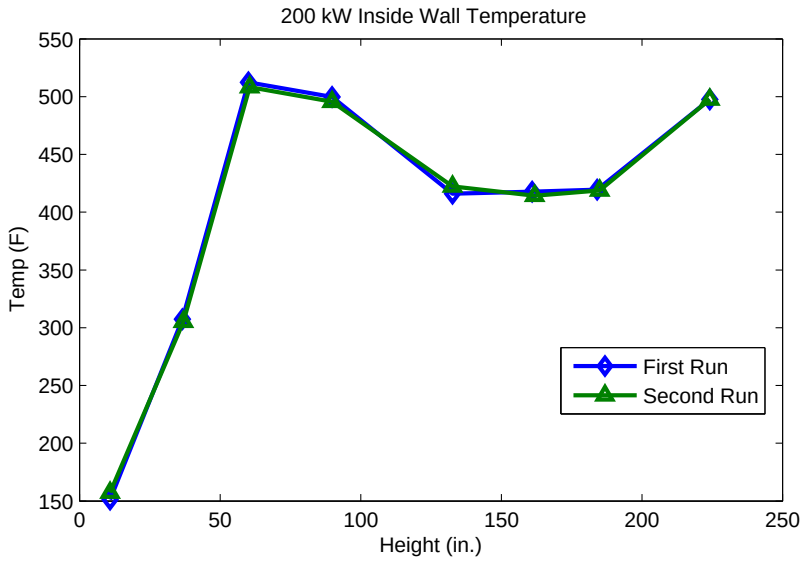

Figure 5.8: Inner Tube Wall Temperature at 200 kW

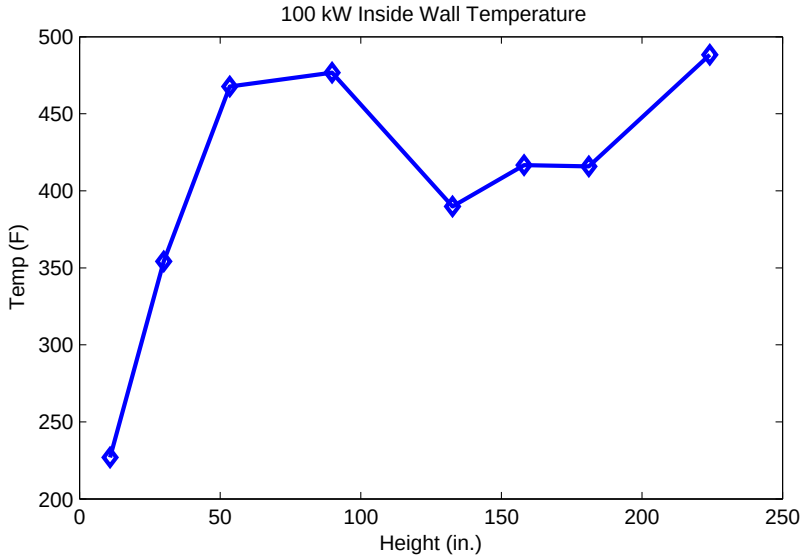

Figure 5.9: Inner Tube Wall Temperature at 100 kW

The heat transfer coefficients calculated across the SG are graphed against the length of the SG tubes. When looking at them, they seem to suggest that the Žukauskas correlation is only reasonable at lower power levels because Figure 5.13 is the only graph where the HTC values look to be even close to the same scale. This is misleading. The calculated HTCs are artificially high because the calculated wall temperature is too high for some cells. This is a product of trying to use a single temperature over such a large length of tubing. Discounting the large spikes at each power level gives a much more reasonable HTC distribution.

Little can be ascertained from this discretized analysis because of the lack of confidence in the calculated HTCs in the boiling region of the SG. At the inlet and exit of the SG tubes, where the flow is single-phase, the HTCs seem reasonable and agree well with global HTC results. The real uncertainty comes from the correlations used inside of the SG tubes. For single-phase flows, both the Schmidt and Mori & Nakayama correlations are well understood and have been proven to work. When it comes to the Modified Chen correlation that is used in the TASS/SMR code and this analysis, there is almost no support except that given by the code developers.

By looking at the HTCs calculated in the single-phase regions, it can be seen that the Žukauskas correlation over predicts the HTC at the local level as well. If more instrumentation were available in the facility, then better wall temperature profiles would be able to be generated without as much guesswork and would be able to be used to accurately solve for the local heat transfer coefficients. Without more information, it is better to use global calculations than to rely on the HTCs generated in this analysis.

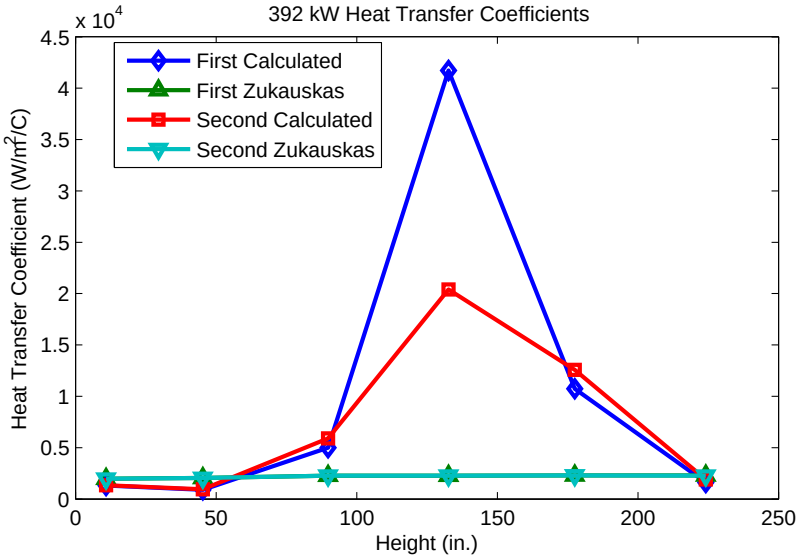

Figure 5.10: Heat Transfer Coefficients Calculated for 392 kW

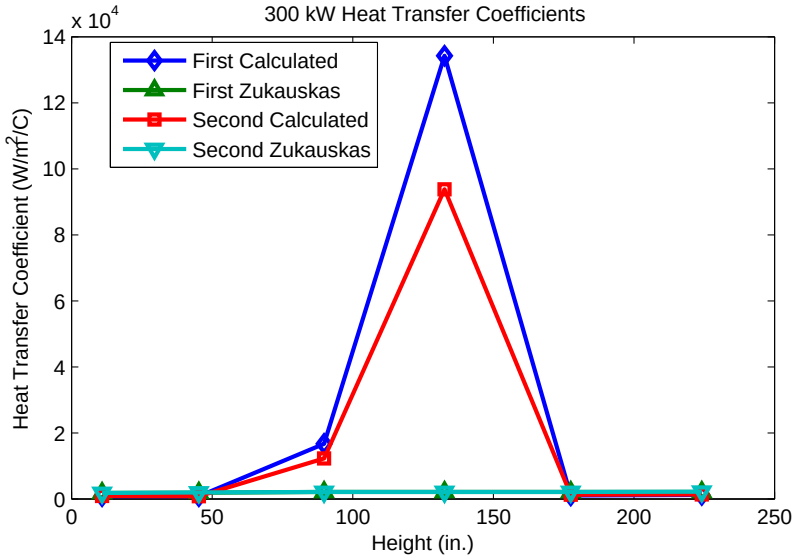

Figure 5.11: Heat Transfer Coefficients Calculated for 300 kW

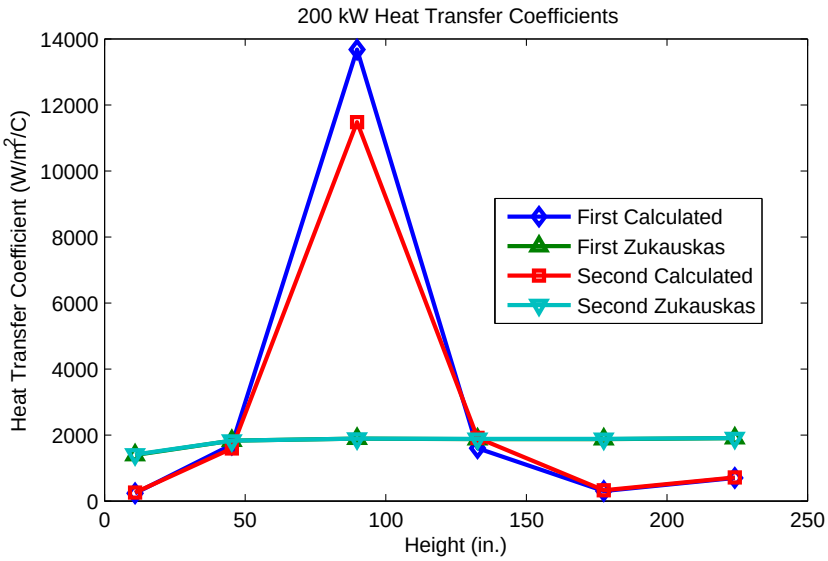

Figure 5.12: Heat Transfer Coefficients Calculated for 200 kW

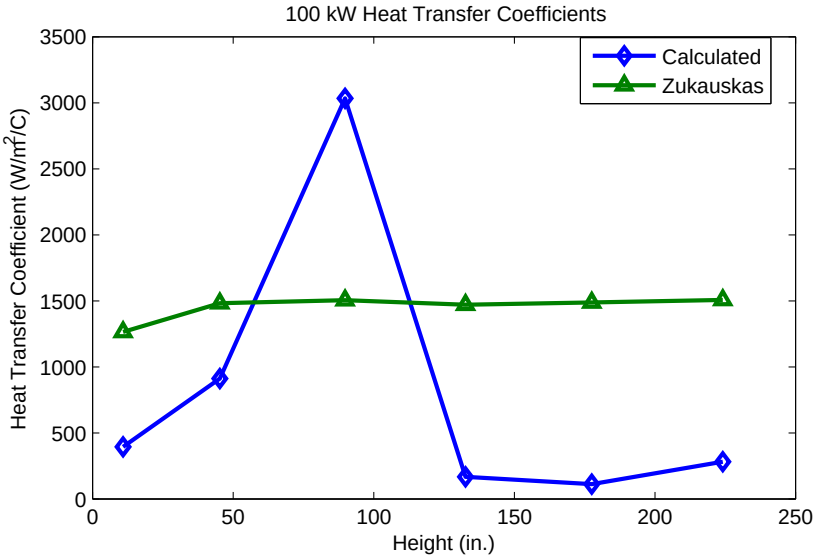

Figure 5.13: Heat Transfer Coefficients Calculated for 100 kW

5.3.1 End Cell Linear Heat Rate Assumption Validation

During the original discretized analysis, an assumption was made that stated that the linear heat rate in transition cells at the end of the SG tubes went to zero. In the Methods chapter, this assumption was discussed thoroughly and found to be lacking support. In an attempt to validate the assumption, a process was proposed to take the HTC in the last cell and back calculate a linear heat rate at the exit of the SG tubes. With this new linear heat rate (q') the heat transfer rate ($\dot{Q}$) was re-weighted over the transition cell and used to recalculate the primary side HTC. It was found that only three of the seven steady state tests required this assumption. When the new HTCs were calculated, they were compared to the originals by looking at the percent difference between the two. All of the differences are cataloged in Table 5.6 and were found to be less than 3%; for the purpose of this analysis, these differences are negligible.

$$\epsilon = \frac{h_{new} - h_{original}}{h_{original}} \tag{5.1}$$

Table 5.6: Error Caused by Linear Heat Rate Assumption

Power(Test #)	**Error**
392 kW(1)	1.61%
300 kW(2)	0.23%
392 kW(2)	2.10%

5.4 Updated Global Analysis

As part of the discretized analysis, a length averaged wall temperature was calculated for each power level, and it may be the most useful data calculated in that analysis. It was used to update the global HTC calculations. The new average wall temperatures are listed in Table 5.7. These wall temperatures, even though calcu-

lated with a large amount of uncertainty, are much more accurate than the guess used in the original global analysis. This is because the guess used was an average of the SG tube inlet and the inlet temperature to the primary side SG region. It is much lower than it should be because of how low the tube inlet temperature is. The tube walls themselves never get close to being that cold in reality, so an average using that temperature will be much too low. The guess also does not account for the length of the different phase regimes in the SG tubes. When the boiling region is higher in the tubes, like at high power, then the average wall temperature should be lower than if the boiling region occurred lower. This is because more of the tubes will be transferring heat to sub-cooled liquid and two-phase flows. The discretized analysis accounted for all of the these considerations and even though there may be little confidence in the local temperatures, themselves their average is still better weighted than the original guess.

Table 5.7: Average SG Tube Outside Wall Temperatures From the Discretized Analysis

Power (kW)	**Temperature (^{o}F)**
392	407.78
300	409.50
200	416.82
100	421.13
200	416.25
300	413.16
392	408.02

The solution for the global heat transfer coefficients using the standard temperature difference with the updated wall temperature are summarized in Table 5.8. Those calculated using the log-mean temperature difference (Equation 4.2) with the updated wall temperature are summarized in Table 5.9.

The heat transfer coefficients calculated in this final analysis are much more promising. In fact, the test runs at 392 kW calculated HTCs that are only a fraction smaller than the correlations. The lower power HTCs did not change

Table 5.8: Updated Global Heat Transfer Coefficients Using Standard Temperature Differences Compared to the Žukauskas Correlation

Power	**Calculated HTC**	**Correlation HTC**
(kW)	(W/m^2C)	(W/m^2C)
392	2031.981	2239.847
300	1475.144	2074.401
200	960.2845	1857.206
100	446.1068	1479.97
200	979.6947	1860.565
300	1528.599	2085.161
392	2016.955	2238.467

Table 5.9: Updated Global Heat Transfer Coefficients Using Log-Mean Temperature Differences Compared to the Žukauskas Correlation

Power	**Calculated HTC**	**Correlation HTC**
(kW)	(W/m^2C)	(W/m^2C)
392	2121.284	2239.847
300	1513.696	2074.401
200	973.1515	1857.206
100	448.0173	1479.97
200	993.2149	1860.565
300	1570.28	2085.161
392	2103.001	2238.467

nearly as much though, which indicates a change in the slope of the coefficient with respect to power level. On average, the Žukauskas correlation is 1.7 times the value calculated with the updated wall temperatures. The difference between the standard and log-mean temperature differences is about the same as the original analysis. Since the log-mean temperature difference calculation is considered to be the better way to use Newton's Law of Cooling, then Table 5.9 is the most accurate calculation of heat transfer coefficients in this analysis.

5.5 Correlation Substitution

In an effort to explore the error in the boiling correlation used in the secondary side the entire problem was redone using the standard Chen Correlation mentioned in the Literature Review. Figure 5.14 though Figure 5.17 show the new inner wall temperatures calculated and Figure 5.18 though Figure 5.21 show the new heat transfer coefficients.

The original Chen correlation uses a version of the Dittus-Boelter correlation for straight pipe convection. [10]

$$h_c = 0.023 Re^{0.8} Pr^{0.4} \quad \frac{k_f}{d} \tag{5.2}$$

This correlation weights the heat transfer in the lower portion of the tubes higher because it causes the Chen correlation to predict the saturated liquid separation from the wall much earlier than the modified correlation. As such, it both reduces the total heat transfer coefficient and pushes it lower in the steam generator.

By looking at the wall temperature and HTC graphs this effect can be seen. The high temperatures are pushed down lower in the SG. It is interesting to note the somewhat strange differences in the graphs in Figure 5.15. This was caused by the transition cell occurring in an inner cell during the first run and in the last cell in the second run. Since different assumptions were made and different correlations used to calculate the temperature the second to last points differ by almost 100F.

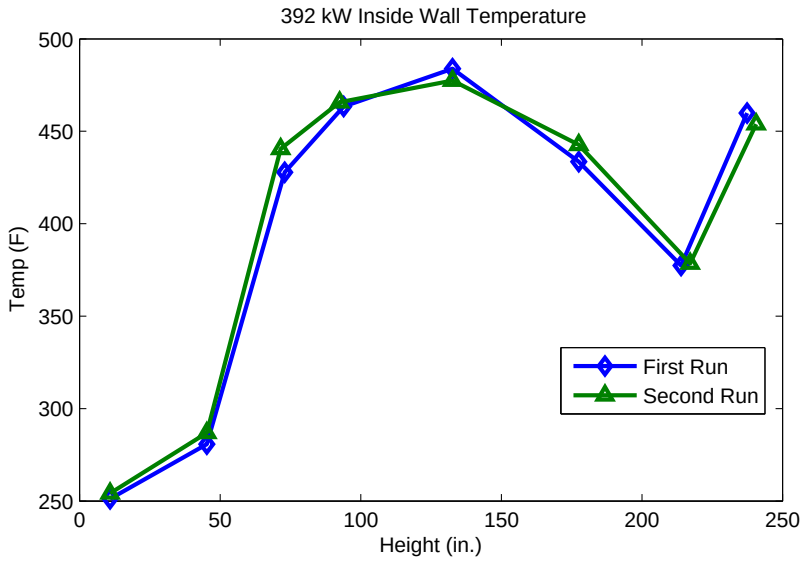

Figure 5.14: Inner Tube Wall Temperature at 392 kW

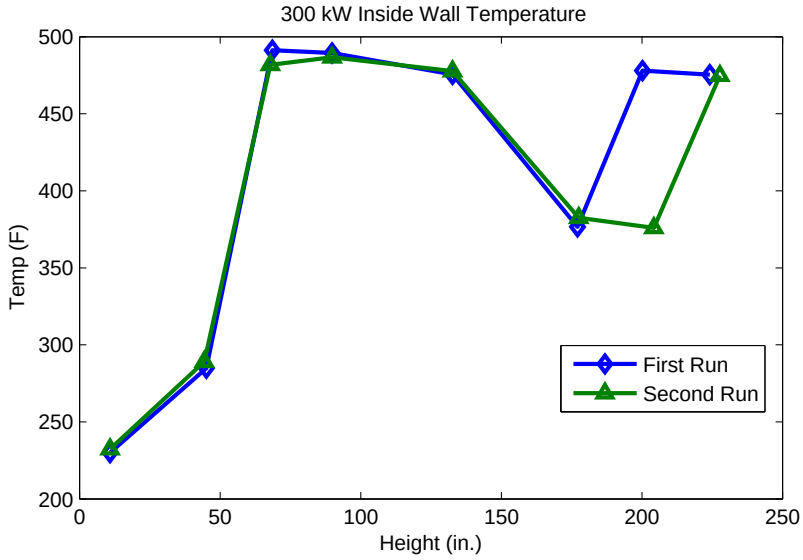

Figure 5.15: Inner Tube Wall Temperature at 300 kW

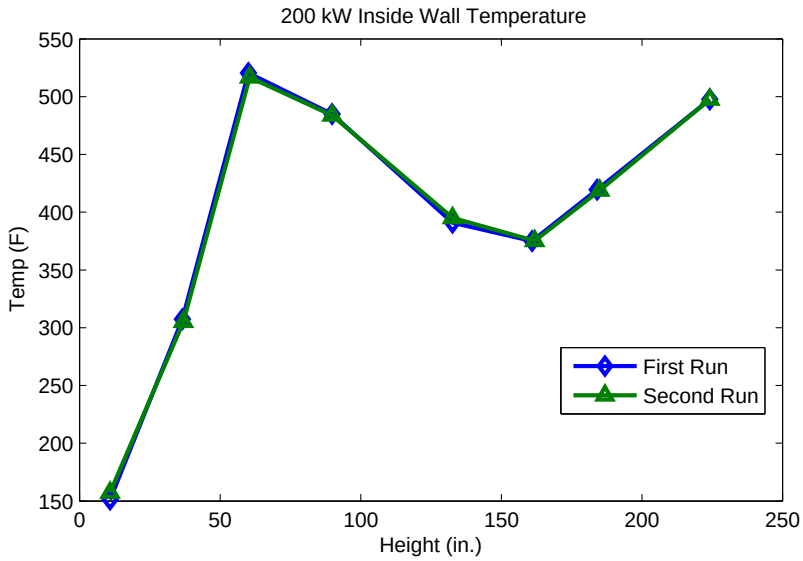

Figure 5.16: Inner Tube Wall Temperature at 200 kW

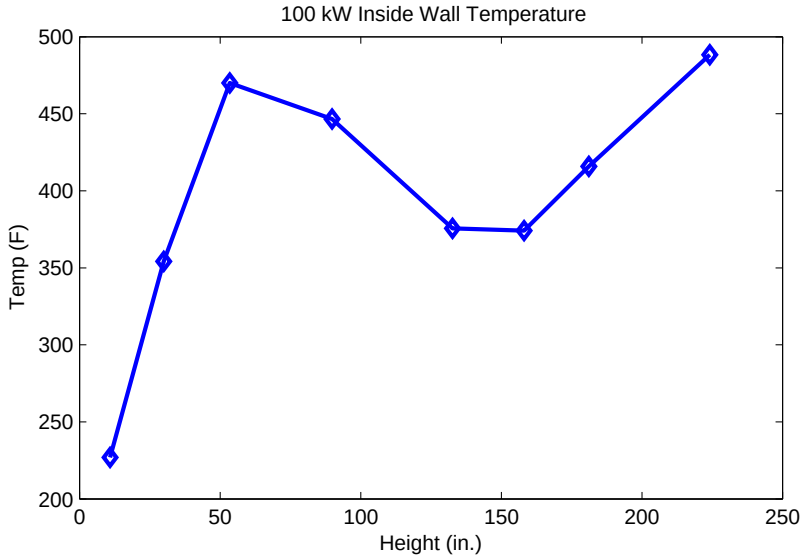

Figure 5.17: Inner Tube Wall Temperature at 100 kW

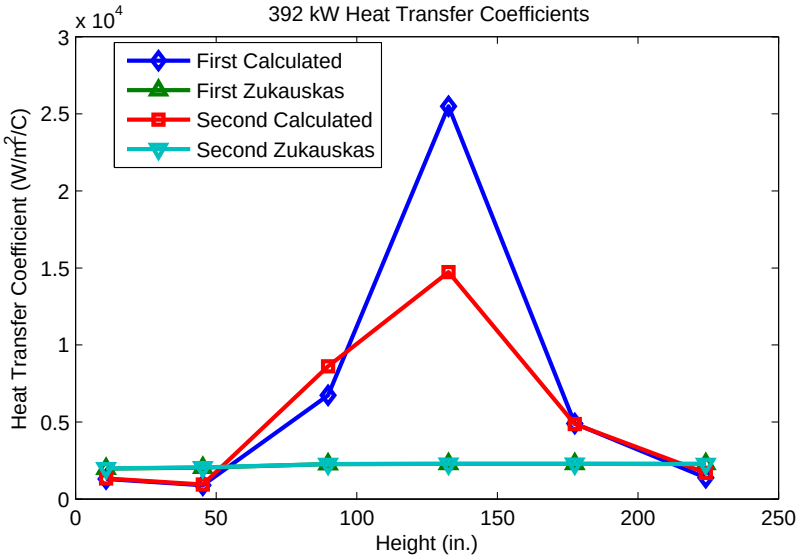

Figure 5.18: Heat Transfer Coefficients Calculated for 392 kW

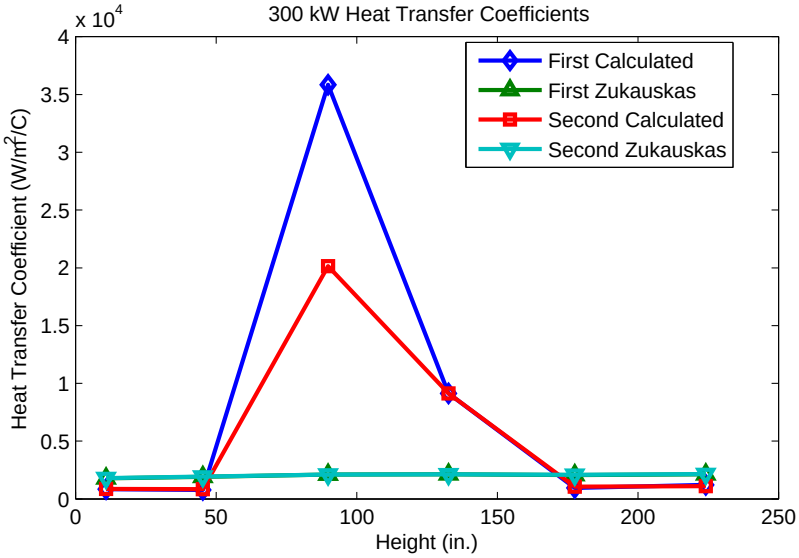

Figure 5.19: Heat Transfer Coefficients Calculated for 300 kW

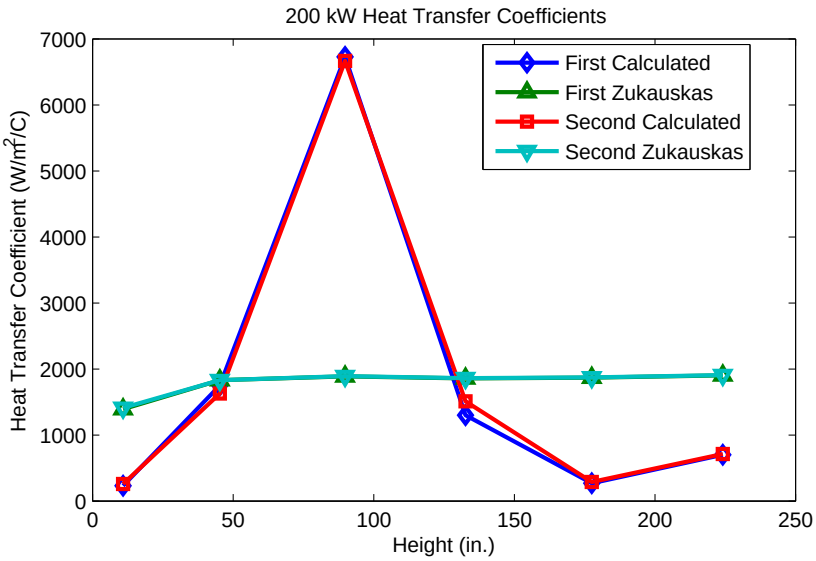

Figure 5.20: Heat Transfer Coefficients Calculated for 200 kW

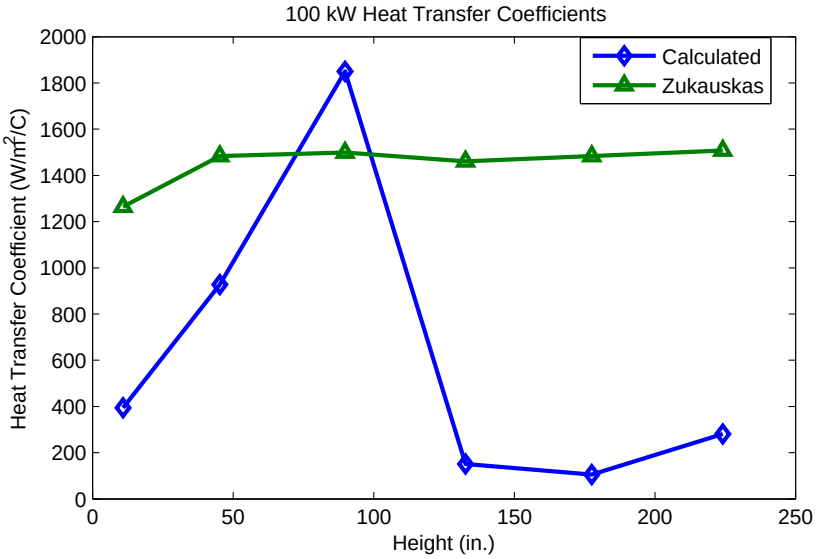

Figure 5.21: Heat Transfer Coefficients Calculated for 100 kW

Chapter 6: Conclusions

From the beginning of this paper, the purpose was to calculate heat transfer correlations with data from the OSU MASLWR Test Facility and compare them with those generated by the Zukauskas correlation. According to engineers in the Korean Atomic Energy Research Institute, their thermal hydraulic systems code, TASS/SMR, used the Zukauskas correlation to analyze the heat transfer coefficient around the helically coiled steam generator modules in the SMART reactor. The hope was that this correlation would be good for modeling helical tube bundles in a natural circulation reactor even though it was designed for straight tube bundles in forced flows.

With the very limited instrumentation from the MASLWR Test Facility's steam generator section, seven sets of data were gathered at steady state operating conditions. The data was averaged over the steady state period to cancel out any noise in the signals and then used to generate an initial global heat transfer analysis. When the same inputs were put into the Zukauskas correlation, it was found to generate much larger heat transfer coefficients.

A local HTC analysis was performed by discretizing the SG into six cells with edges at the instrumentation heights and using simplified conservation of energy equations to find the bulk fluid temperatures inside the SG tubes. With those temperatures, the tube wall temperatures were solved for and used to calculate the heat transfer coefficients by using the wall temperatures and the known primary fluid temperatures. The heat transfer coefficients calculated were very erratic because of the extremely large cell size required by the instrumentation configuration. With more temperature points, this study would have been able to find much better heat transfer coefficients to be compared with the Zukauskas correlation.

It was observed that the internal tube correlations miscalculated the heat transfer in the boiling region. More calculations and data will need to be used in the future to test the Modified Chen correlation for its applicability to the MASLWR SG.

One good piece of information was found in the discretized analysis: the total length averaged wall temperature. The new average wall temperatures were used to update the global analysis and find better heat transfer coefficients. At the highest power, the HTC was found to be only a small fraction smaller than what was calculated by the Zukauskas correlation. The lower powers were still largely different, but the higher the power and flow rates, the closer the correlation was. This is thought to be because the higher flow rates simulated forced flow conditions.

Although the focus of this project, the discretized analysis, did not provide quality results, it has yielded many insightful experiences for the author. It is hoped that a future analysis with better instrumentation will be able to do a more accurate discretized computation and prove whether the Zukauskas correlation is valid for helical coils in natural circulation flow.

Bibliography

[1] Hee-Kyung Kim, Soo Hyoung Kim, Young-Jong Chung, and Hyeon-Soo Kim. Thermal-hydraulic analysis of SMART steam generator tube rupture using TASS/SMR-S code. *Annals of Nuclear Energy*, 55:331–340, 2013.

[2] Yasuo Mori and Wataru Nakayama. Study on forced convective heat transfer in curved pipes (2nd report, turbulent region). *International Journal of Heat and Mass Transfer*, 10:37–59, 1967.

[3] W.R. Dean. Note on the Motion of Fluid in a Curved Pipe. *Philosophical Magazine*, 4:208–223, 1927.

[4] W.R. Dean. The Stream-line Motion of Fluid in a Curved Pipe. *Philosophical Magazine*, 5:673–695, 1928.

[5] H. Ito. Laminar Flow in Curved Pipes. *ZAMM*, 49, 1969.

[6] R.A. Seban and E.F. McLaughlin. Heat transfer in tube coils with laminar and turbulent flow. *International Journal of Heat and Mass Transfer*, 6:387–395, 1963.

[7] Tomasz Sobota. Experimental Prediction of Heat Transfer Correlations in Heat Exchangers. *Developments in Heat Transfer*, 2011.

[8] Yasuo Mori and Wataru Nakayama. Study on forced convective heat transfer in curved pipes (1st report, laminar region). *International Journal of Heat and Mass Transfer*, 8:67–82, 1965.

[9] Ali Owhadi, Kenneth J. Bell, and Berry Crain Jr. Forced convection boiling inside helically-coiled tubes. *International Journal of Heat and Mass Transfer*, 11:1779–1793, December 1968.

[10] John C. Chen. Correlation for Boiling Heat Transfer to Saturated Fluids in Convective Flow. *I&EC Process Design and Development*, 5(3):322–329, July 1966.

[11] Dvanahalli G. Prabhanjan, Timothy J. Rennie, and G.S. Vijaya Raghavan. Natural convection heat transfer from helical coiled tubes. *International Journal of Thermal Sciences*, 43:359–365, 2004.

[12] G.Y. Kanevets and A.A. Politykina. Heat Transfer in Crossflow Over Bundles of Coiled Heat-Exchange Tubes. *Applied Thermal Sciences*, 2:38–41, 1989.

[13] A. Žukauskas. Heat Transfer from Tubes in Crossflow. *Advances in Heat Transfer*, 8:93–160, 1972.

[14] Soo Hyung Yang, Soo Hyung Kim, Young-Jong Chung, Hyun-Sik Park, and Keung Koo Kim. Experimental validation of the helical steam generator model in the TASS/SMR code. *Annals of Nuclear Energy*, 35:49–59, 2008.

[15] Young-Jong Chung, Soo Hyoung Kim, and Hee-Cheol Kim. Thermal hydraulic analysis of SMART for heat removal transients by a secondary system. *Nuclear Engineering and Design*, 225:257–270, 2003.

[16] In Sub Jun, Kyoo Hwan Bae, Young Jong Chung, and Won Jae Lee. Validation of the TASS/SMR-S Code for the Core Heat Transfer Model on the Steady Experimental Conditions. *Journal of Energy and Power Engineering*, 6:338–345, 2012.

[17] Ji-Han Chun, Kyu-Hyung Lee, and Young-Jong Chung. Assessment and SMART application of system analysis design code, TASS/SMR-S for SBLOCA. *Nuclear Engineering and Design*, 254:291–299, 2013.

[18] H.K. Forster and N. Zuber. Dynamics of Vapor Bubbles and Boiling Heat Transfer. *AIChE Journal*, 1(4):531–535, December 1955.

[19] Trond A. Bjornard and Peter Griffith. PWR Blowdown Heat Transfer. *Thermal and Hydraulic Aspects of Nuclear Reactor Safety*, pages 17–41, 1977.

[20] R.W. Lockhart and R.C. Martinelli. Proposed correlation of data for isothermal two-phase, two-component flow in pipes. *Chemical Engineering Progress*, 45(1):39–48, January 1949.

[21] Frank P. Incropera, David P. DeWitt, Theodore L. Bergman, and Adrienne S. Lavine. *Fundamentals of Heat and Mass Transfer*. John Wiley & Sons, Inc., New Jersey, 6 edition, 2007.

[22] Neil E. Todreas and Mujid S. Kazimi. *Nuclear Systems I.* Taylor & Francis Group, New York, 1990.

[23] Kendall Atkinson and Weimin Han. *Elementary Numerical Analysis.* John Wiley & Sons, Inc., New Jersey, 3 edition, 2004.

[24] P.S. Srinivasan, S.S. Nandapurkar, and F.A. Holland. Pressure drop and heat transfer in coils. *The Chemical Engineer*, 218:113–119, May 1968.